Economic Geology, v. 105, pp. 395–416

Fluid Inclusion Constraints on the Genesis of Gold in the Darasun District (Eastern Transbaikalia), Russia

Vsevolod Yu. Prokofiev,[1,2] Paolo S. Garofalo,[†,3] Nikolay S. Bortnikov,[2] Vladimir A. Kovalenker,[3] Lidiya D. Zorina,[4] Dmitriy V. Grichuk,[1] and Sofiya L. Selektor[5]

[1]*Department of Geology, Lomonosov Moscow State University, Vorob'evy gory, Moscow, 119899 Russia*

[2]*Institute of Geology of Ore Deposits, Petrography, Mineralogy, and Geochemistry, Russian Academy of Sciences, Staromonetnyi per. 35, Moscow, 119017 Russia*

[3]*Dipartimento di Scienze della Terra e Geologico-Ambientale, Università di Bologna, Ambientali, Italy*

[4]*Vinogradov Institute of Geochemistry and Analytical Chemistry, Siberian Division, Russian Academy of Sciences, ul. Favorskogo 1a, Irkutsk, 664033 Russia*

[5]*Frumkin Institute of Physical Chemistry and Electrochemystry RAS, Moscow, Russia*

Abstract

Darasun, Teremkyn, and Talatui are neighboring deposits in the Darasun gold district of Transbaikalia (Russia) that are hosted by Middle-Late Jurassic subduction-related porphyry intrusions and dikes. Darasun consists of vertically extensive, steeply dipping Au mineralized veins and zones, spatially related to a K-rich granodiorite-porphyry intrusion. Within the deposit are also pipelike bodies of tourmaline sulfide hydrothermal breccias. Teremkyn consists of gently and steeply dipping veins and zones, always associated with felsic dikes comagmatic with the Darasun intrusion. Talatui consists of variably shaped mineralized zones systematically associated with dikes of different compositions and with the host Middle-Late Jurassic granite porphyry. A large proportion of both veins and mineralized zones in these deposits consists of sulfide and oxide minerals, with pyrite and arsenopyrite mostly present at Darasun and Teremkyn and pyrite, magnetite, and hematite present at Talaui. The three deposits host also a large number of sulfosalt, bismuth, oxide, and telluride minerals. Gold of variable purity occurs as free nuggets or hosted by opaque phases. The gangue mineralogy is similar in the three deposits and includes commonly quartz, tourmaline, and calcite.

Microthermometry and microchemical analyses of fluid inclusions with petrographic and compositional data on ore minerals constrain the stages of ore deposition in the district. At room temperature, the entrapped fluids are of four compositional types: (1) multiphase, with a vapor bubble, liquid, and one or more solids; (2) liquid-vapor aqueous; (3a) vapor-rich with a small proportion of liquid and rare solids, and also (3b) vapor-rich with a small proportion of aqueous liquid and carbonic liquid. Types (1) and (3) or (2) and (3) coexist within the same assemblages and are present mostly in paragenetically early quartz, whereas the type (2) fluid within later quartz, sphalerite, and calcite shows consistent phase proportions. At Darasun and Teremkyn, type (2) fluid is the main ore fluid, but all fluid types are associated with gold deposition at Talatui.

Microthermometric measurements from all fluid types show a range of phase transitions that vary systematically at the deposit scale. At Darasun and Teremkyn, coexisting types (1) and (3) and types (2) and (3) homogenize into the vapor and liquid states, respectively, within the same 290° to 460°C range. The corresponding bulk salinities vary between 0.7 and 44.8 wt percent NaCl equiv. In contrast, at Talatui coexisting types (1) and (3) and types (2) and (3) homogenize into the vapor and liquid phases and show a distribution of $T_{h(total)}$ and bulk salinities between about 300° and 610°C and 0.9 and 48 wt % NaCl equiv, respectively. Mass spectrometric and chromatographic data from bulk samples show that the main-stage ore fluid in the three deposits varies compositionally according to location within the district. In detail, Cl, Na, K, Cs, Br, Sr, Rb, Mn, and Tl are relatively enriched in the Talatui fluid, whereas CO_2, CH_4, HCO, Cu, Pb, Sb, Fe, Hg, and REE are enriched at Darasun and Teremkyn or show no systematic variations. Au concentrations vary within the 0.01- to 3-g/t range at Darasun and Teremkyn, whereas at Talatui values do not exceed 0.4 g/t.

The salinities and homogenization temperatures of the main-stage ore fluids types (1), (2), and (3) are typical of the intrusion-related class of gold deposits. This suggests a dominant magmatic component of the ore fluid during the first stages of mineral precipitation and a magmatic derivation of gold itself in the district. Phase separation was active during the early stages of ore deposition and took place between about 600° to 400°C at Talatui and 450° to 300°C at Teremkyn and Darasun at pressures of 10 to 160 MPa (i.e., 1- to 2.5-km depth). This explains the systematic distribution of ore minerals and fluid chemistry within and around the orebodies. Gold precipitation took place within the three deposits during both early-stage phase separation (Talatui and Darasun) and main-stage ore formation. Microchemical data of fluid inclusions show that the ore fluid was characterized by Au/Cu ratios between 15 and 35 (units: g/t vs. wt %). This range is five orders of magnitude higher than that determined for porphyry Cu deposits (~$1{\cdot}10^{-4}$, Ulrich et al., 1999) and compares well with the range of Au/Cu ratios measured in the most fractionated melt hosting the Timbarra intrusion-related deposit of Australia (20–200, Mustard et al., 2006). Hence, similar to porphyry Cu systems, the Au/Cu ratios of the ore fluid at Darasun could have been controlled by the fundamental Au/Cu ratio of the magmatic source rock.

† Corresponding author: e-mail, paolo.garofalo@unibo.it

0361-0128/10/3880/395-22

Submitted: February 15, 2009
Accepted: January 28, 2010

The petrographic evidence for an association between gold and galena and the evidence for consistently high concentrations of Pb, Zn, and Fe in the fluid inclusions suggest that a fraction of the fluid that deposited the orebodies did not always reach saturation in gold and other ore minerals during the early magmatic-hydrothermal stage. We speculate that a fraction of the ore fluid was transported through the orebodies and dispersed at lower temperatures into the outer fringes of the deposits, where they formed the documented galena-sphalerite halo around the Darasun stock.

Introduction

The Darasun goldfield is a mining district in Transbaikalia, Russia, that is of relevant geologic and economic importance (Sakharova, 1968, 1969, 1972; Timofeyevsky, 1972; Lyakhov and Dmitriev, 1975; Zorina et al., 1991; Yurgenson and Yurgenson, 1995; Prokof'ev et al., 2000, 2004, 2007; Bortnikov, 2006). The district is named after the largest deposit of the region, the Darasun gold mine that has been productive for more than a century (Timofeyevsky, 1972; Safonov, 1997; Bortnikov, 2006). Darasun was discovered in 1861 and produced 118 metric tons (t) from underground operations and an additional 40 t from surface (gold placer) operations. Production stopped between 1996 and 2002 and restarted with higher gold prices in 2003.

The most recent classification schemes identify Darasun as a greenstone-hosted, quartz-carbonate Au vein deposit (Gosselin and Dubé, 2005; Yakubchuk et al., 2005). Such schemes do not consider, however, recent data gathered at Darasun and on companion deposits of the district; therefore, they do not consider possible genetic links with the granitoid intrusions that occur in the region. The Darasun goldfield hosts literally hundreds of economic and subeconomic Au-bearing occurrences, all of which show spatial and temporal associations with rocks of calc-alkaline affinity (Prokof'ev et al., 2000). Here, we present a set of petrographic, microchemical, and fluid inclusion data on three deposits of the goldfield, namely Darasun, Talatui, and Teremkyn (Fig. 1). Darasun and Teremkyn are companion deposits hosted by the same granodiorite porphyry intrusion, whereas Talatui is located 12 km northwest of Darasun and shares with them several geological and geochemical similarities. Given the overall dimensions of this mineralized system, knowledge of the genesis of these three deposits provides valuable insight into the nature of transport and deposition of gold within the district. From the record presented here, we propose that gold in the three deposits was provided by a common magmatic source whose Au/Cu ratio was comparable to that of the ore fluid.

Geologic Background

The Darasun, Teremkyn, and Talatui gold mines are located in the Chita area of the eastern Transbaikal region, 70 km southwest of the Mongolian-Okhotsk suture zone generated by the collision between the Mongolian and Siberian continents at the end of the Mesozoic. The tectonic evolution of the region is complicated by a sequence of thrusting, folding, and magmatism that lasted for about 50 m.y., from the Early and/or Middle Jurassic to the end of the Jurassic. This region hosts more than 30 identified gold deposits of variable economic relevance (Zorin et al., 1998, 2001), half of which have characteristics similar to Darasun and occur close to, or along, structural lineaments of various order. A detailed account of the tectonic history of eastern Transbaikalia and its relationships with the regional minerogenesis is provided by Zorin et al. (2001), and an account of the geologic history of the Darasun area and of the geochemical features of its deposits is found in literature that is summarized in the paragraphs below.

The Darasun goldfield is located within a block having a complex tectonic structure and consisting of Paleozoic magmatic rocks. The ultramafic and mafic rocks of the Early Paleozoic Kruchinsky Complex (Pz_1) are the oldest of such rocks (Fig. 1). They consist mainly of pyroxene-hornblende, hornblende and olivine gabbros, and minor serpentinitic pyroxenites, plagioclase dunites, peridotites, and anorthosites. According to some authors (Kazimirovsky et al., 1992) these rocks formed after fractional crystallization of a single mafic-ultramafic melt of mantle derivation, whose composition was similar to that of a subalkaline picrite. These rocks differ from ophiolites due to their high alkalinity, their relatively high concentrations of K, Ti, Rb, Sr, and the depletion of MgO, CaO and FeO. They are similar to rift basalts (Kuzmin, 1985; Kazimirovsky et al., 1992) and may be remnants of the Early Paleozoic oceanic crust that formed the Mongolian-Okhotsk ocean 462 ± 110 Ma ago (Fedorov et al., 1980; whole-rock Rb-Sr age).

These gabbroic rocks are intruded to the south and southeast by the Middle Paleozoic Krestovsky Complex (Pz_2), consisting of diorites, quartz diorites, granodiorites, granites, and aplites dated at 320 to 316 Ma (Kazimirovsky et al., 1992; whole-rock Rb-Sr dating). The Late Paleozoic-early Mesozoic leucogranites, granodiorites, syenites, and granosyenites of the Olyokminsky Complex (Pz_3) represent an extension to the northeast and southeast of the Krestovsky Complex (Fig. 1). Leucogranites are depleted in the majority of metals except for Pb, Rb, Th, and U and are similar to the palingenic granites of the Russian literature (Kazimirovsky et al., 1998).

A Triassic granitoid intrusion (234 ± 8 Ma, biotite K-Ar age) forms the Amanansky Complex to the northwest of Darasun (Rublev et al., 1985). The dominant lithology is a subalkaline granodiorite, with minor biotite-amphibole-two feldspar diorite, granosyenite, granites, alaskite granite. The Middle Jurassic-Early Cretaceous Amudzhikan-Sretensky Complex (J_2-K_1) is the youngest magmatic suite of the region and includes subvolcanic and effusive high potassium rocks showing a large range of compositions: dikes and stocks of porphyritic diorites, granosyenite, syenite, and granite porphyries, plagioporphyry dikes, felsites, felsite porphyries, trachybasalts, trachyandesites, latites, trachydacites, rhyodacites, quartz porphyries, and rhyolites. This suite occurs in close spatial association with the orebodies and is volumetrically small (Fig. 1). Within the Darasun deposit, it forms a high K, calc-alkaline series, characterized by the occurrence of magnetite inclusions within plagioclase and biotite, variable total Fe (Σ_{Fe} = 3.32–8.12), high LILE contents, and by anomalous enrichments in Ag, Au, Mo, and W.

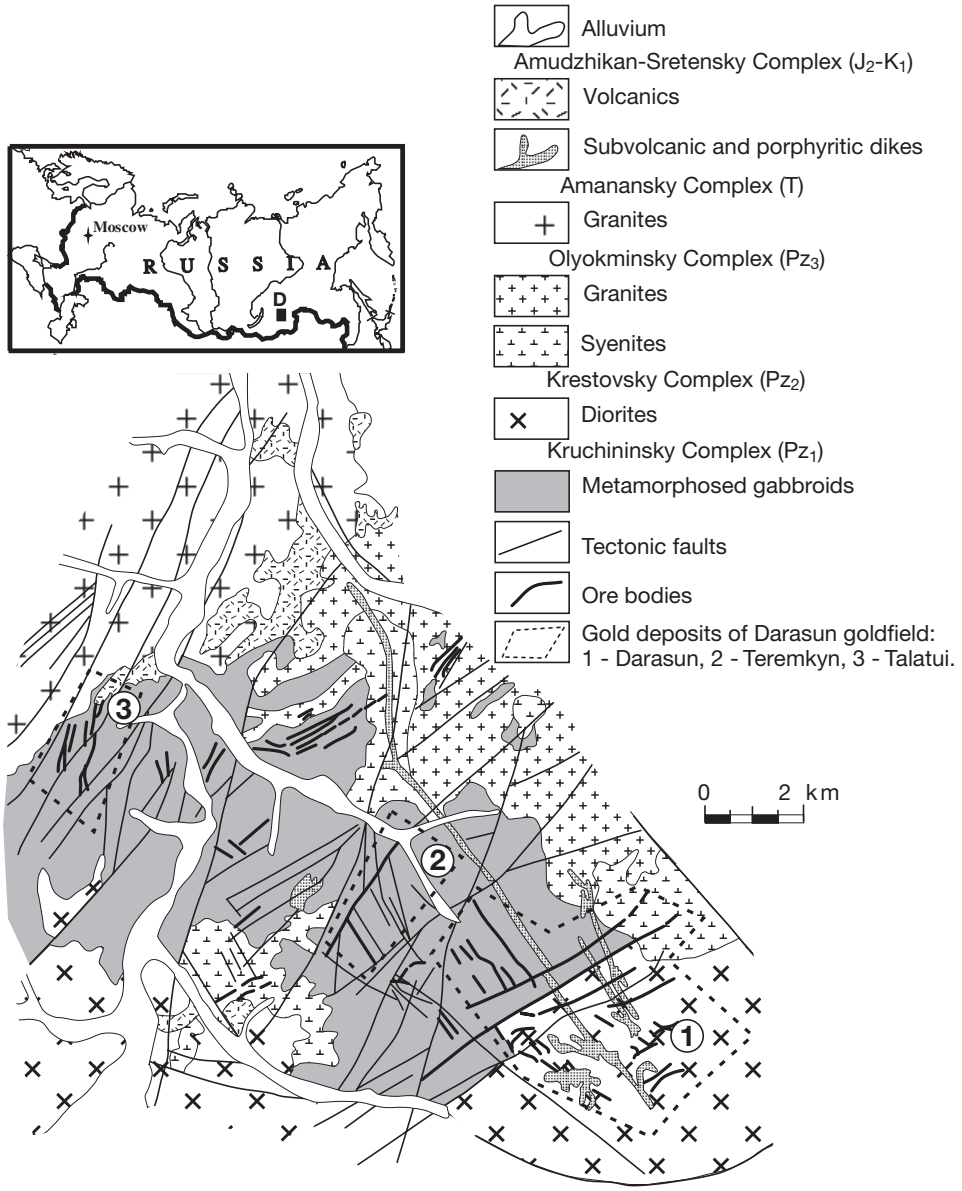

FIG. 1. Location of the Darasun goldfield (D) and geologic sketch of the district. The dotted lines mark the extent of the mine properties. 1 = Darasun, 2 = Teremkyn, 3 = Talatui. Modified after Prokof'ev et al. (2006).

Orebodies and subvolcanic rocks are located in the same brittle and ductile structures, showing that structural control was important for both emplacement of the magmatic suite and the Au mineralization. The deposits are located within and around the porphyry stocks and associated apophyses and can be traced from hundreds of meters to kilometers downdip or along strike. At Darasun and Teremkyn, veins and ore shoots are found within a system of northeast to northwest trending faults (Fig. 1) with sharp walls and alteration haloes. At Talatui, the orebodies are represented by northwest-trending ore shoots with transitional boundaries and spatially irregular (with an en echelon arrangement) alteration zones. In all deposits, gold grades are clearly controlled by local pinch-swell structures and fractures. We have not observed clear cross-cutting relationships between orebodies and host rocks in the district; therefore, we cannot provide geologic evidence for relative timing of the hydrothermal event. K-Ar isotope and Rb-Sr dating of biotite, plagioclase, and whole rock, respectively (Table 1), shows, however, that hydrothermal alteration of the wall rocks took place between 165 and 145 Ma (Timofeyevsky, 1972; Pakhol'chenko et al., 1987), which is consistent with the Middle Jurassic-Early Cretaceous age of the granodiorite porphyries of the Amudzhikan-Sretensky Complex in the region (193–109 Ma, Rublev et al., 1985, biotite K-Ar age). More recent Sm-Nd dating of vein tourmaline, arsenopyrite, and calcite from Darasun constrained gold deposition at 100 ± 18 Ma (Prokof'ev et al., 2006), i.e., to the final stages of emplacement of the granodiorite porphyries.

The Darasun deposit

Darasun includes more than 200 steeply dipping gold-mineralized quartz veins spatially related to the K-rich granodiorite

TABLE 1. Isotopic Ages Determined for the Amudzhikan-Sretensky Complex

Sample	Method	Age (Ma)	Reference
Quartz diorite porphyries, pipelike	K-Ar	174 ± 10	Timofeevskii (1972)
Granodiorite porphyries, stocklike	K-Ar	170 ± 10	Timofeevskii (1972)
Syenite porphyries, central dikelike body	K-Ar	169 ± 5	Prokof'ev et al. (2000)
Effusive analogues of granodiotite porphyries	K-Ar	165 ± 7	Timofeevskii (1972)
Volcanic glass, pipelike	K-Ar	162 ± 5	Prokof'ev et al. (2000)
Pekhstein, nappe	K-Ar	160 ± 10	Timofeevskii (1972)
Granite porphyries, stocklike	K-Ar	160 ± 5	Prokof'ev et al. (2000)
Diorite porphyries, dike	K-Ar	156 ± 5	Prokof'ev et al. (2000)
Quartz diorite porphyries, dike	K-Ar	145 ± 4	Prokof'ev et al. (2000)
Hydrothermally altered rocks, near arsenopyrite-rich vein	K-Ar	165 ± 7	Timofeevskii (1972)
Propylitic alteration, near apy-rich vein	Rb-Sr	150 ± 8	Pakholchenko et al. (1987)
Quartz-muscovite-carbonate alteration halo, near arsenopyrite vein	Rb-Sr	144 ± 10	Pakholchenko et al. (1987)
Granodiorite porphyries, stocklike and dike	K-Ar	193–109	Rublev et al. (1985)
Tourmaline-arsenopyrite-calcite vein	Sm-Nd	100 ± 18	Prokof'ev et al. (2006)

porphyry intrusion of the Amudzhikan-Sretensky Complex (J_2-K_1, Fig. 2). Besides explosive breccias (Timofeyevsky, 1972), a disseminated ore generated by a high-temperature and highly saline ore fluid has been recently documented (Prokof'ev et al., 2008). The host rocks are the Early Paleozoic gabbroids and Middle to Early Paleozoic granitoids. Intense propylitic alteration predates ore formation, whereas a sericite-chlorite-quartz-pyrite-carbonate alteration coeval with ore deposition is observed close to the veins. The actual shape of the Darasun stock at the present day erosional surface is extremely irregular, marked by a large number of apophyses (Fig. 2). The rocks that form this stock derived from a high K, calc-alkaline magma of latitic composition (Tauson et al., 1987). The orebodies are located within and around the granodiorite porphyries and their dikelike apophyses. Timofeyevsky (1972) was the first to document the local concentric zoning of the Darasun orebodies and their regular distribution relative to the stocks (Fig. 2). He found a quartz-tourmaline assemblage in the center of the bodies and a more distal pyrite-arsenopyrite assemblage. Veins with average As content equal to 0.5 wt percent are typical of the central part, whereas those containing 10 wt percent or more As are located away from the center. A galena-sphalerite assemblage is distributed in variable amounts within the distal parts of the orebodies and forms a halo around the stock. The geochemical anomalies of B and other ore elements form a series of concentric zones around the stock (Timofeyevsky, 1972; Tauson et al., 1987).

A set of quartz sulfide veins and mineralized zones are located in a system of northeast- and northwest-trending fractures, although postmineralization displacements and pinching and swelling complicate this setting. Vein length is up to 2 km along strike and 1.0 to 1.2 km along dip, with a width that varies from 5 to 20 cm. The length of the ore shoots ranges from about 100 to 1,000 m, and variable textures and fabrics are typical for ores in this deposit (Timofeyevsky, 1972). Textures vary from fine to coarse grained and the crystals are predominantly euhedral. Massive, lenticular, lenslike, crustlike, and brecciated textures were documented. Ores contain 40 to 60 vol percent of sulfides (Sakharova, 1968, 1969, 1972; Timofeyevsky, 1972) and contain more than 100 mineral species. Main phases are pyrite, arsenopyrite, chalcopyrite, pyrrhotite, tennantite-tetrahedrite, bournonite, galena, sphalerite, native gold, quartz, carbonates, and tourmaline. A notable feature of the deposit is the widespread occurrence of Pb, Cu, Sb, Bi, Ag, and As sulfosalts and telluride minerals. The assemblages chalcopyrite, tetrahedrite-tennantite; chalcopyrite, pyrrhotite, gold (Au grade: 20–300 g/t); pyrite, arsenopyrite, gold (Au grade: 25–35 g/t); as well as the Ag-Cu-Te-Bi–bearing assemblage are of major commercial interest and occur mainly in ore shoots.

Paragenetic studies (Sakharova, 1968, 1969; Timofeyevsky, 1972) show that the Darasun deposit formed during three stages of mineral precipitation (Fig. 3). During the early stage, a tourmaline, pyrite, quartz assemblage, and a pyrite, arsenopyrite, quartz, siderite, chalcopyrite (with sphalerite and anhydrite inclusion), and native gold assemblage formed. The following main stage includes pyrite, chalcopyrite, galena, sphalerite, quartz, dolomite, Bi tellurides, pyrrhotite, Cu, Pb, Sb, Bi, Ag, and As sulfosalts, Bi and Ag tellurides, most native gold, and Pb and Ag sulfoantimonides, stibnite, and calcite. During a late (postore) stage, the quartz-calcite veins formed.

The Teremkyn deposit

Located 5 km northwest of Darasun, the Teremkyn deposit consists of a series of Au-bearing tourmaline-quartz sulfide veins and zones of disseminated ore (Fig. 4). Gold is visible in the orebodies and occurs as inclusions with volumetrically minor Ag, Cu, Bi, Pb, Zn, and Sb minerals. Host rocks are the Early Paleozoic gabbroids of the Kruchinsky Complex (Pz_1) and the Late Paleozoic-early Mesozoic granitoids of the Olyokminsky Complex (Pz_3). The deposit itself is defined by the intersection between a system of faults and the granodiorite porphyry of the Amudzhikan-Sretensky Complex (J_2-K_1), which is in turn part of the Darasun Suite. The different types of volcanic glass within the dikes and the felsites are characterized by anomalously high B contents (i.e., up to 295 and 325 g/t, respectively) compared to other volcanic rocks of the Transbaikal region (Antipin et al., 1985). Dikes and Au mineralized veins occur together in three levels of the deposit, forming an important association. Another relevant association is that between mineralization and hydrothermal breccias (Kulikova et al., 1996).

A distinguishing feature of the orebodies at Teremkyn is the extremely irregular distribution of gold but within clearly defined ore shoots. The highest gold grades are found within

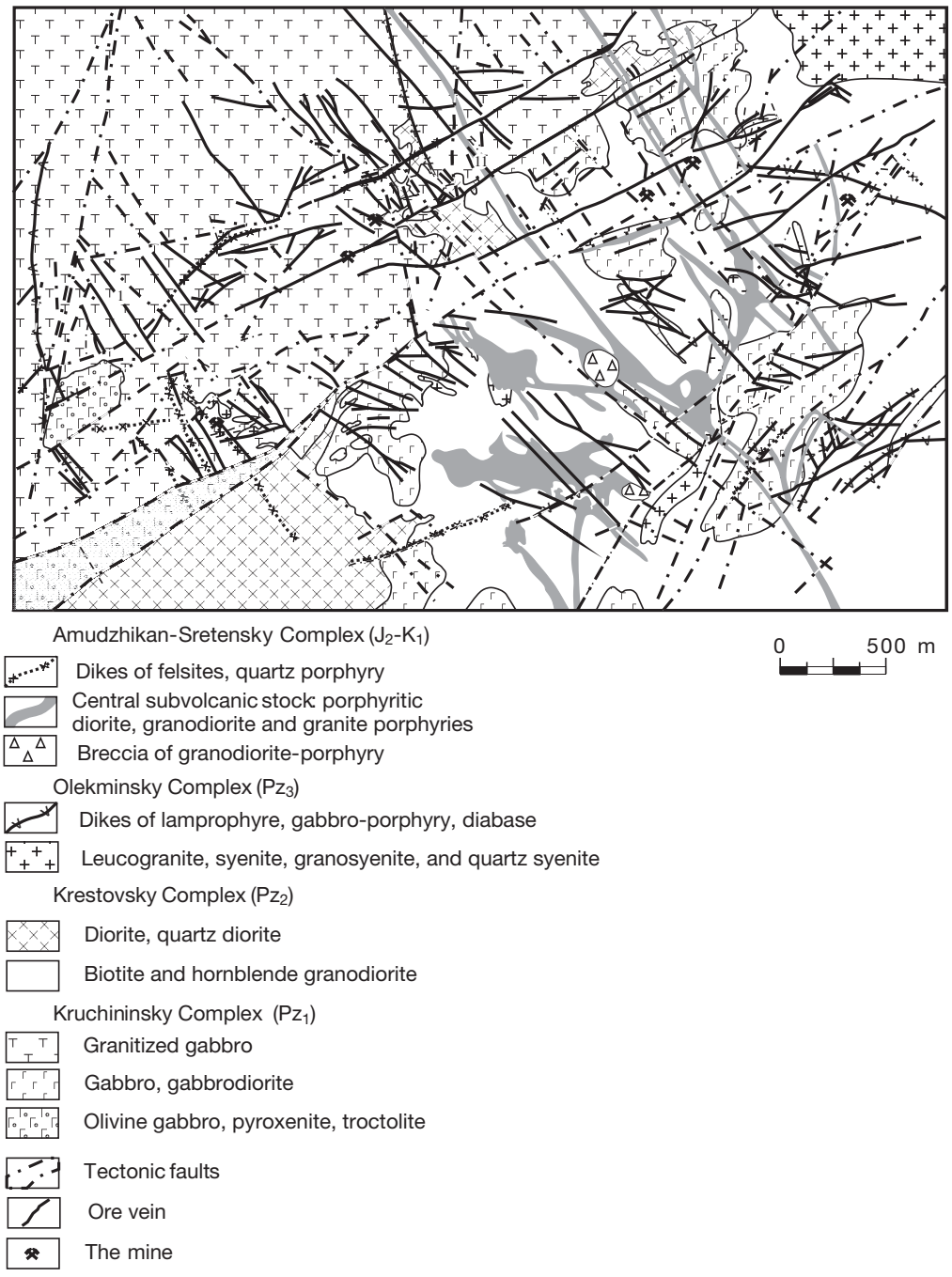

FIG. 2. Geologic map of the Darasun deposit. Based on unpublished data of Yu.A. Aferov, N.M. Kalinichenko, R.A. Amosov, and I.B. Semerkov.

northeast-trending veins dipping 50° to the south, as well as in south- and northeast-trending veins dipping 10° to 30° to the south. Ore shoots occur in areas of pinch and swell, where vein density is the highest. This feature is so characteristic of Teremkyn that accurate reserve evaluations have been carried out along the east-, northeast-, and north-trending structures, especially at their intersections.

The vein paragenesis of Teremkyn is not defined with the same detail as for Darasun, although preliminary reports show the presence of quartz, tourmaline, pyrite, arsenopyrite, chalcopyrite, sphalerite, galena, marcasite, pyrrhotite, native gold, electrum, bismuth minerals (native bismuth, bismuthine, aikinite, cosalite, matildite, and tetradymite), bournonite, lead sulfoantimonites, carbonate, chalcedony, zeolite, and fluorite (Zorina et al., 1991; Yurgenson and Yurgenson, 1995; Prokof'ev et al., 2004). Such association is essentially undistinguishable from that of Darasun. Textural relationships show that massive quartz and rare molybdenite predate gold precipitation within the veins (Zorina et al., 1991). Coeval with this stage of precipitation is the intense propylitic alteration of the host rocks.

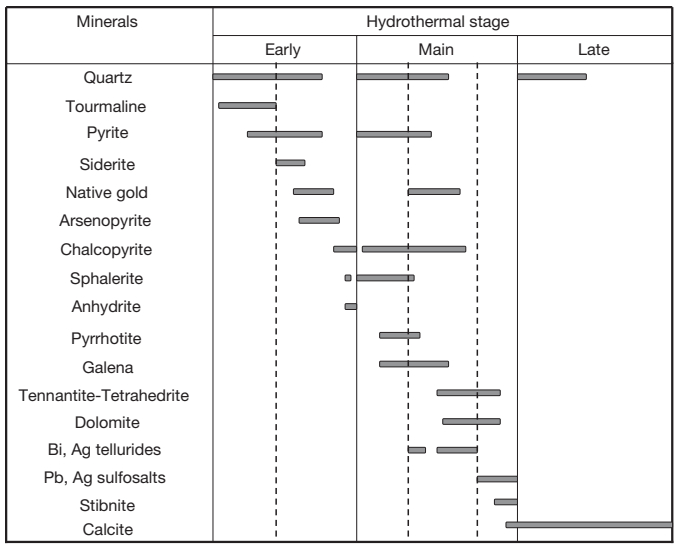

FIG. 3. Generalized sequence of ore mineral formation at Darasun.

We distinguish three stages of vein formation at Teremkyn (Fig. 5). The first stage corresponds to the formation of the (a) quartz, tourmaline, pyrite, and (b) quartz and arsenopyrite assemblages. The second stage, volumetrically most important, corresponds to the generation of the (c) quartz, pyrite, chalcopyrite, native gold, (d) quartz, chalcopyrite, sphalerite, galena, matildite, native gold, (e) quartz, chalcopyrite, cubanite, pyrrhotite, native gold, and (f) quartz, bournonite, tetradymite, joseite, pilsenite, galena, native bismuth, bismuthine, aikinite, cosalite, native gold, tetrahedrite, and calcite assemblages. The third quartz-carbonate assemblage postdates ore formation. Gold grains are mostly round in shape, up to 50 μm in size, and form together with quartz, chalcopyrite, sphalerite, galena, and bismuth minerals. In some veins, the early quartz-tourmaline and quartz-pyrite assemblages are replaced by the quartz-sulfide-gold and the late quartz-carbonate assemblages. Sulfides provide the cement of quartz-tourmaline and pyrite fragments of hydrothermal breccias.

The quartz-sericite-carbonate and chlorite-carbonate-talc types of hydrothermal alteration of the host rocks are coeval

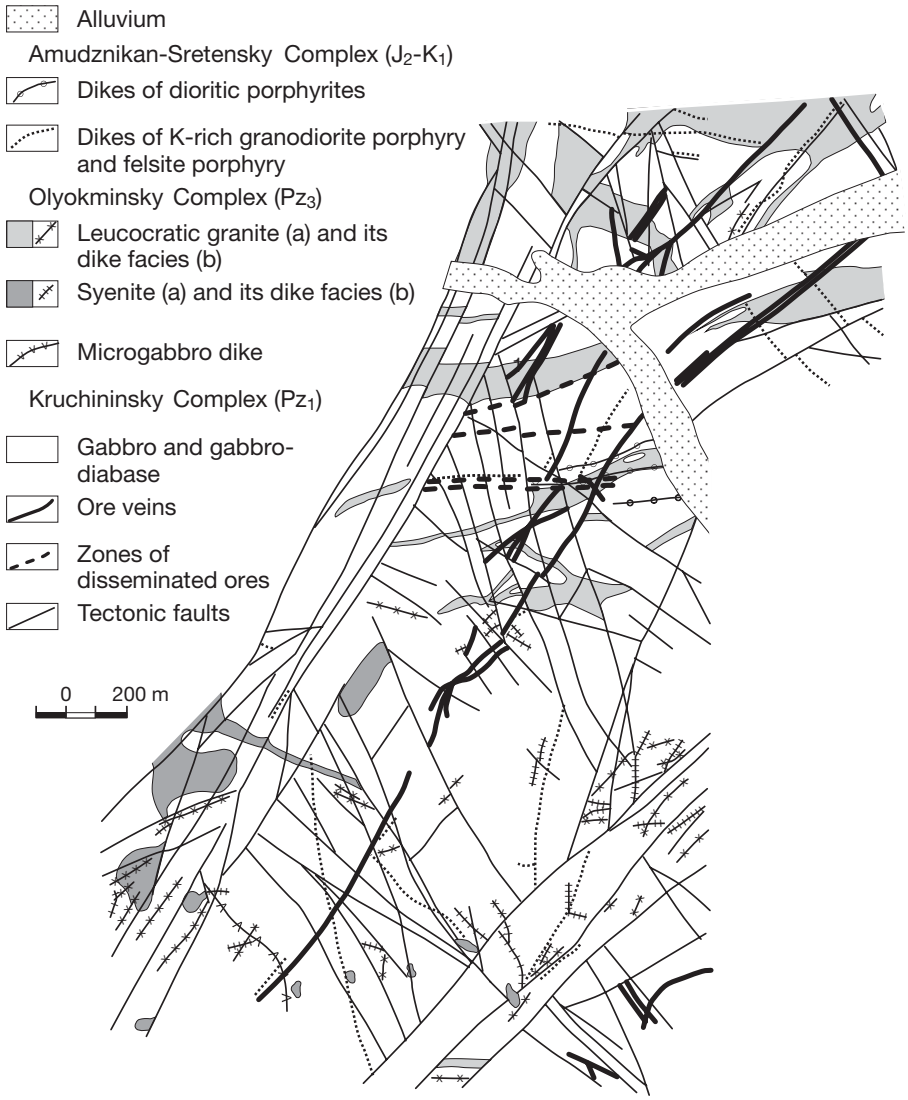

FIG. 4. Geologic map of the Teremkyn deposit. Modified after Prokofiev et al. (2004).

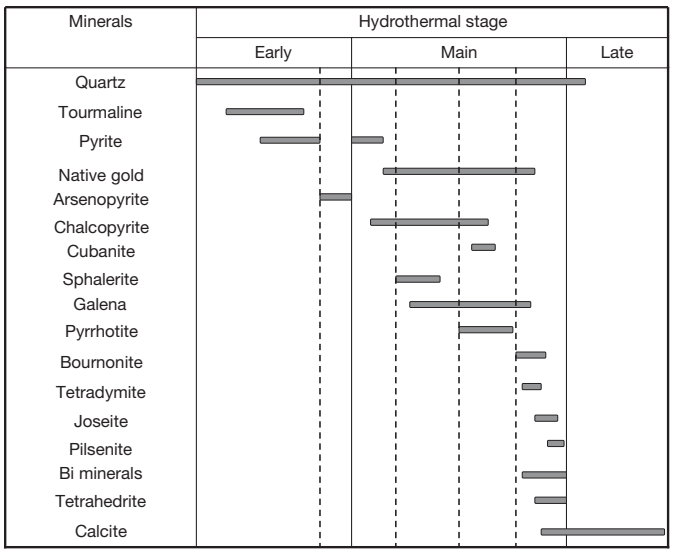

FIG. 5. Generalized sequence of ore mineral formation at Teremkyn.

with the main stage of mineral precipitation and were dated at 144 ± 10 Ma (Pakhol'chenko et al., 1987), which is appreciably younger than that of the corresponding alteration at Darasun (i.e., 165 ± 7 Ma; Timofeyevsky, 1972).

The Talatui gold deposit

The Talatui deposit is located 8 km northwest of Darasun (Fig. 6). Its orebodies are hosted by the hydrothermally altered gabbro, gabbro-monzonite, gabbrodiorite, and diorite of the Early Kruchininsky Complex (Pz_1), which are in turn crosscut by Middle Jurassic-Early Cretaceous dikes and stocklike intrusions of porphyritic diorite, granite porphyry, granodiorite porphyry, quartz porphyry, and lamprophyres compositions of the Amudzhikan-Sretensky Complex (J_2-K_1; Fig. 6). The host rocks are in contact with the Triassic granitoids of the Amanansky Complex (T) to the northwest and with the Late Paleozoic (Pz_3) leucogranite, syenite, and granosyenite of the Olyokminsky Complex to the northeast. To the south, they are in contact with Middle Paleozoic diorite and granodiorite of the Krestovsky Complex (Pz_2).

The gabbroic host rocks show high concentrations of alkali metals ($\Sigma K_2O + Na_2O$ = 4–5 wt %) owing to their hydrothermal alteration. Textural analysis shows clear evidence for this outer alteration, which generated the outer orthoclase, quartz, epidote, magnetite, rutile, phlogopite, and tourmaline; the intermediate orthoclase, actinolite, phlogopite, pyrite, anhydrite, barite, and quartz; and the inner adularia, chlorite, sericite, quartz, and calcite mineral assemblages (Prokof'ev et al., 2007). The alteration zones are arranged in an en echelon fashion around the orebodies, although they are complicated by numerous faults. The orebodies are northwest trending, mostly vein shaped with subordinate lenticular zones (Fig. 6). Their thickness varies from 0.25 to 20 m and their contacts with the host rocks are transitional (they were identified by detailed sampling). Underground data allow the orebodies to be traced for 2,000 m along strike and for 200 to 500 m downdip. They are characterized by alternations of 4- to 20-m-long pinches and 40- to 120-m-long swells. The latter are controlled by the local geometry of the tectonic contacts or by the presence of transverse faults extending to the northwest. The highest gold grades occur where the orebodies intersect these transverse faults.

With an average grade of 9.5 g/t, gold is the main ore component of Talatui (Benevolskiy, 2002), although it occurs associated with a suite of other commodities like Ag (6.4 g/t), Cu (0.16 wt %), W (0.084 wt %), and Bi (0.014 wt %). The major vein minerals are K-feldspar, magnetite, and quartz, which sum up to more than 50 vol percent (Prokof'ev et al., 2007). The sulfides are represented mainly by pyrite and chalcopyrite and make up more than 15 percent of the vein volume, whereas epidote, chlorite, tourmaline, and phlogopite are minor phases. Scheelite, sphalerite, titanite, hematite, goethite, and hercynite are all trace vein phases, and galena, siegenite, matildite, pilsenite, hessite, wittichenite, anhydrite, barite, wolframite, and zircon (but also gypsum and pyrrhotite) are found as small inclusions within the sulfides. Replacement of magnetite after hematite (i.e., magnetite pseudomorph over platy hematite) is a typical ore texture. The gangue minerals include K-feldspar, quartz, epidote, tourmaline, biotite, phlogopite, sericite, actinolite, tremolite, clinochlore, chalcedony, and carbonates. By analogy with the Darasun deposit, we identify three stages of vein formation at Talatui (Fig. 7): an early stage during which the assemblage orthoclase, quartz, epidote, magnetite, tourmaline, phlogopite, scheelite, native gold, pyrite, molybdenite formed; a main stage coincident with precipitation of quartz, tourmaline, muscovite, pyrite, anhydrite, barite, hematite, chalcopyrite, native gold, molybdenite, sphalerite, and quartz; and a late (postore) stage with chalcopyrite, bornite, pilsenite, hessite, matildite, quartz, and calcite.

Association between gold and ore minerals in the district

District-scale observations show that at Darasun the highest Au grades occur with the main-stage mineral assemblage (range: 20–300 g/t) and microchemical data (Table 2) show a variable degree of gold purity (fineness: 590–997‰), with Ag contents in the 0.9 to 40.8 wt percent range and Hg, Sb, and Te forming important minor constituents. At Darasun, gold is typically found in association with pyrite, arsenopyrite, chalcopyrite, galena, tellurides of Bi and Hg, and quartz (Fig. 8a-d), whereas at Teremkyn gold occurs in association with pyrite, pyrrotite, Bi sulfosalts, and quartz (Fig. 8e-h). At Talatui, a paragenetically early, high-purity gold (fineness: 964–997‰) is associated with rutile, magnetite, scheelite, and K-feldspar (Fig. 8i-l), whereas a paragenetically late gold (fineness: 777–874‰) occurs as small inclusions (up to 10 μm in size) within magnetite, pyrite, and chalcopyrite. These minerals are in turn cut by thin veinlets of electrum (fineness: 440‰).

Another typical feature of Darasun, Teremkyn, and Talatui is the relative abundance and variety of tellurium minerals in textural equilibrium with pyrite, chalcopyrite, and gold (Table 3). At Darasun (Fig. 9) the assemblage is represented by petzite ($AuAg_3Te_2$), pilsenite (Bi_4Te_3), tsumoite (Bi_2Te_2), tellurobismuthite (Bi_2Te_3), tetradymite (Bi_2Te_2S), alexite ($PbBi_2Te_2S_2$), hessite (Ag_2Te), and volynskite ($AgBiTe_2$). At Teremkyn, minor pilsenite, hessite, matildite ($AgBiS_2$), hedleyite (Te_2Bi), tetradymite, sulphotellurides of Bi, joseite-A and -B (A: Bi_4TeS_2; B: Bi_4Te_2S), and vikingite ($Ag_5Pb_8Bi_{13}S_{30}$) make a peculiar

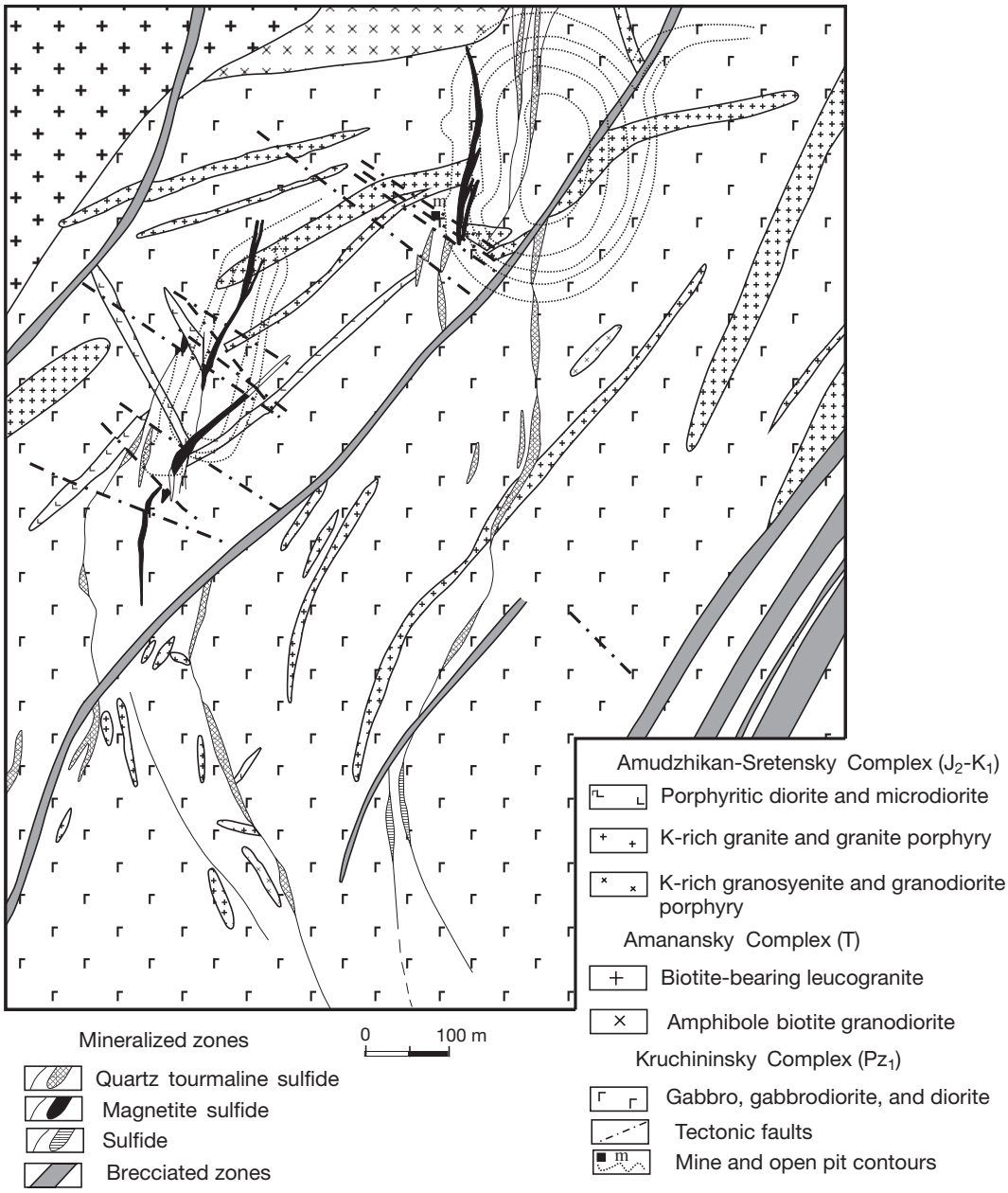

FIG. 6. Geologic sketch of the Talatui deposit. Modified after Prokofiev et al. (2007).

aggregate of small-grained crystals in textural equilibrium. At Talatui, minor pilsenite, hessite, and matildite make an aggregate of small-grained crystals in textural equilibrium.

Fluid Inclusion Data

Fluid inclusion types

In the three deposits, fluid inclusions have a regular or negative crystal shape (sensu: Bakker and Diamond, 2006) and are found within vein quartz from all stages of Au deposition. In the most favorable early- and main-stage samples, these inclusions mark the growth bands of euhedral quartz (Fig. 10a), i.e., they identify stages of fluid entrapment coeval with quartz and gold precipitation (primary inclusions). Less commonly, inclusions occur within microfractures not exceeding the limits of quartz crystals (pseudosecondary inclusions) or within microfractures crosscutting all phases (secondary inclusions). We focused our work on the primary and pseudosecondary fluid inclusions hosted in the early quartz and also within stage (2) and (3) quartz, sphalerite, and calcite in order to constrain all possible stages of ore deposition (Table 4). The fluids found within these samples are described by four compositional types: (1) multiphase inclusions (solid-liquid-vapor, S-L-V) containing a vapor bubble, an aqueous liquid, and one or more solids represented by cubic crystals or occasional opaque ore minerals (Fig. 10d, f-g); (2) liquid-vapor (L-V) aqueous inclusions (Fig. 10b-c, e, h-i); and (3) vapor-rich (V-rich) inclusions with a thin rim of aqueous

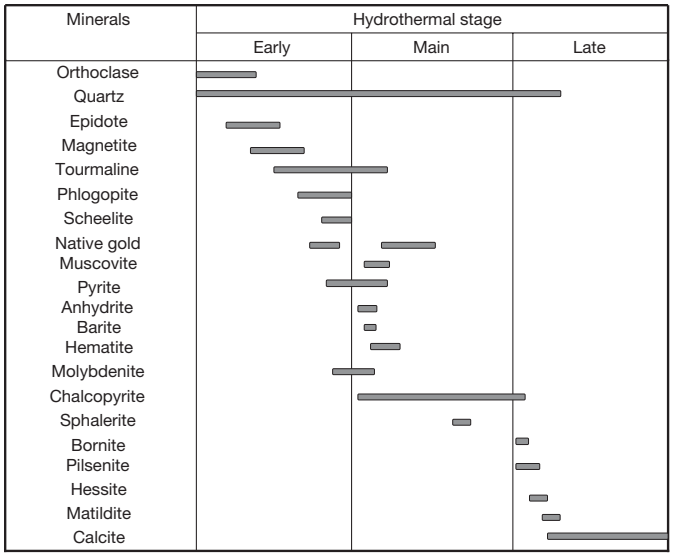

FIG. 7. Generalized paragenetic sequence of the Talatui deposit.

liquid and occasional cubic crystals (Fig. 10d-e, k, type 3a), or relatively rare, three-phase vapor inclusions (liquid-liquid-vapor) made of an aqueous liquid, a carbonic liquid, and a carbonic vapor at room temperature (Fig. 10l, type 3b). It is quite common to find inclusion types (1) to (3) within the same sample, within the same quartz crystal, or even within the same growth band (Fig. 10a-b), which suggests, at least locally, a heterogeneous state of the ore fluid at the time of Au deposition. Inclusion types (1) to (3) are found also within the quartz of the hydrothermal alteration haloes. Only type (2), two-phase inclusions are observed in late-stage minerals.

Methods

The work was carried out on about 400 groups of inclusions entrapped within quartz, sphalerite, anhydrite, and calcite from 150 doubly polished plates of the three deposits, which totals over 2,300 fluid inclusions documenting all stages of ore deposition (Table 4). The host minerals record the early and main stages of ore formation and are paragenetically coeval with Au precipitation (Fig. 8c). Hence, our fluid inclusion database provides some constraints but is limited relative to a study of groups of cogenetic inclusions along individual growth planes or microfractures, i.e., of "Fluid Inclusion Assemblages" (cf. Goldstein, 2003). As a result, our data do not provide a detailed reconstruction of the changes of ore fluid properties as a function of time of entrapment within individual host minerals (e.g., from the beginning to the end of early quartz precipitation). However,

TABLE 2. Chemical Composition of Au in the Darasun Goldfield (wt %)

Analysis	Au	Ag	Cu	Fe	Bi	Te	Hg	Sb	Total	Fineness (‰)
					Darasun					
1	89.82	10.28	-	-	-	0.06	-	0.11	100.27	896
2	89.33	11.30	0.06	-	0.15	0.20	0.01	0.17	101.22	883
3	89.01	11.36	0.30	-	-	0.10	-	0.05	100.82	883
4	76.41	22.14	-	0.01	0.06	0.07	0.46	0.02	99.17	770
5	72.26	26.62	-	0.01	-	0.12	1.05	-	100.06	722
6	70.88	29.31	0.01	0.01	0.36	0.14	-	-	100.71	704
7	59.78	40.82	0.06	0.25	-	0.14	0.35	-	101.40	590
					Teremkyn					
8	92.91	6.86	0.04	-	0.23	0.06	-	-	100.10	928
9	91.26	8.35	0.04	-	0.35	0.05	-	0.15	100.20	911
10	90.14	8.51	0.08	-	0.46	-	0.19	-	99.38	907
11	88.64	11.62	-	-	0.27	-	-	0.02	100.55	882
12	83.76	16.90	0.13	-	0.06	0.03			100.88	830
13	79.57	20.44	0.45	-	-	0.04	0.59	-	101.09	787
14	66.34	34.05	0.38	-	0.04	0.10	0.29	0.03	101.23	655
					Talatui					
15	99.22	0.09	0.12	0.03	0.01	0.05	-	0.03	99.55	997
16	97.83	1.92	0.15	0.27	0.35	0.13	-	0.02	100.67	972
17	95.76	2.95	0.09	0.52	-	0.10	0.13	0.17	99.72	960
18	96.29	2.31	0.19	1.65	0.11	-	-	0.08	100.63	957
19	85.76	12.88	0.10	0.08	0.17	0.15	0.32	-	99.46	862
20	86.00	12.78	0.07	0.08	0.15	0.13	0.78	0.08	100.07	859
21	78.25	20.17	0.88	0.68	0.12	0.03	-	-	100.13	781
22	78.00	20.79	0.50	0.86	0.16	0.04	-	-	100.35	777

Notes: The chemical compositions of gold and other ore minerals (Table 3) were determined at the Institute of Geochemistry and Analytical Chemistry, RAS (analyst N.N. Kononkova) on a Camebax SX 100 X-ray microprobe (filament current: 30 nA; accelerating voltage: 20 kV; beam diameter: 2–5 m); measurements were performed using the Pb*M*, S*K*, Bi*M*, Ag*L*, Au*L*, Zn*K*, Fe*K*, Cd*L*, Mn*K*, Cu*K*, Hg*L*, Se*L* analytical lines, and concentrations were calculated using PAP corrections; the limit of detection is 0.02 wt % for most elements, while measurement uncertainty is ±2% and ~20% for major and trace elements, respectively; - = below limit of detection; these analyses have been carried out following a preliminary petrographic study of polished thin sections and in parallel with semiquantitative microanalysis of the associated silicate vein phases, which were carried out with a JSM5300 and JSM5610LV SEM equipped with a LINK ISIS EDS (acceleration voltage: 25 kV; analyst: N.V. Trubkin)

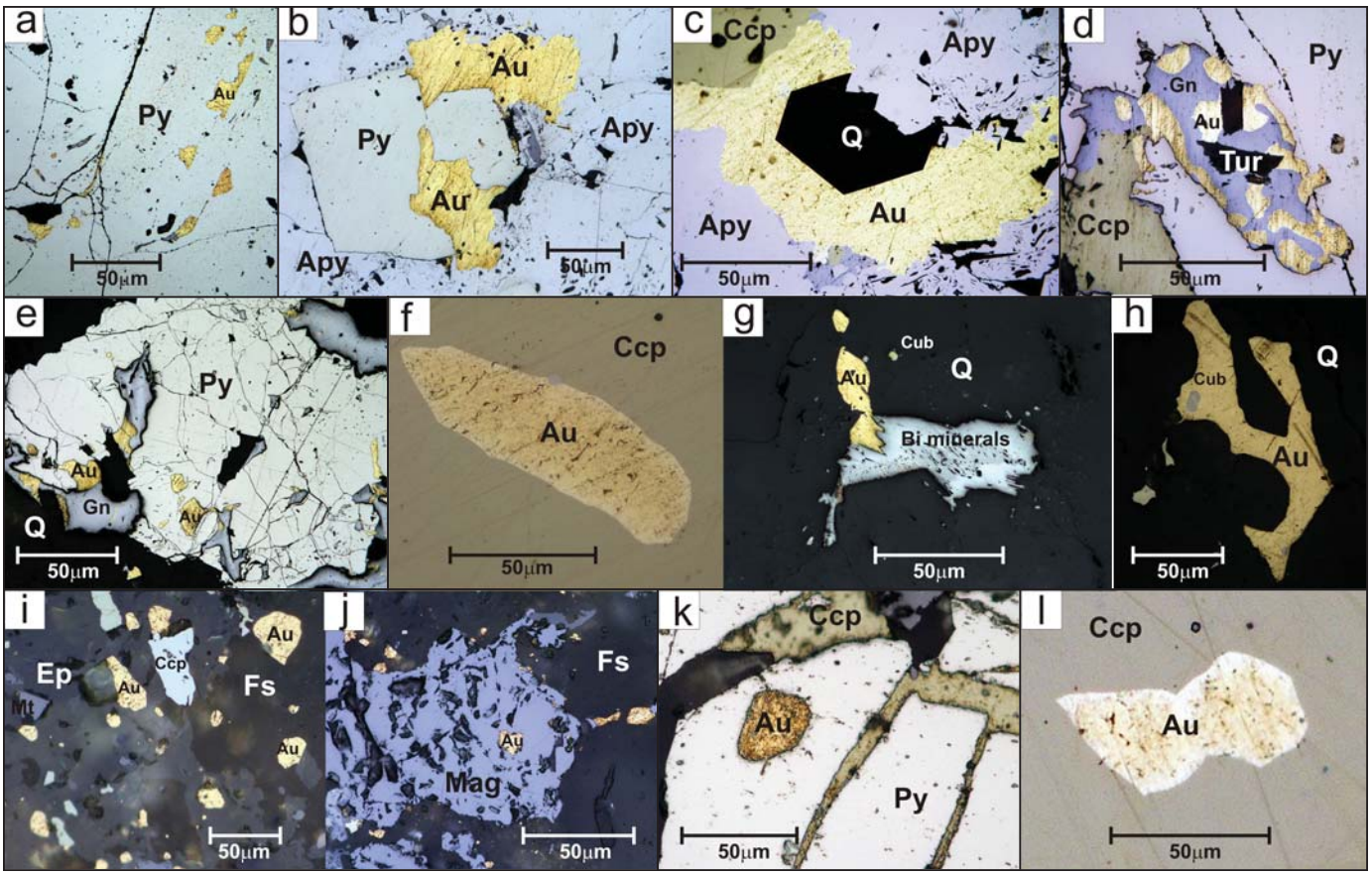

FIG. 8. Representative gold occurrences in the Darasun goldfield (all photomicrographs from polished blocks in reflected light). Darasun deposit: gold associated with early-stage pyrite (ab) and arsenopyrite (b); gold associated with main-stage chalcopyrite (c) and galena (d). Teremkyn deposit: gold associated with early-stage pyrite (e) and chalcopyrite (f); gold associated with main-stage Bi minerals and cubanite (gh) and quartz (h). Talatui deposit: gold associated with early-stage magnetite, K-feldspar, and epidote (ij); gold associated with main-stage pyrite (k) and chalcopyrite (l). Length of the scale bar is 50 μm in all panels. Abbreviations: Au = gold, Apy = arsenopyrite, Bi min = bismuth minerals, Ccp = chalcopyrite, Cub = cubanite, Ep = epidote, Fs = K-feldspar, Gn = galena, Py = pyrite, Q = quartz, Tur = tourmaline. All mineral abbreviations follow Kretz (1983).

the data do allow discrimination between distinct ore fluids from the same stage of vein formation (e.g., fluid types (1) and (2) within early quartz) or between groups of inclusions hosting the same fluid type but from distinct stages of vein formation (e.g., type (2) inclusions from main- and late-stage quartz).

Fluid inclusion microthermometry was performed on a Linkam THMSG-600 heating-freezing stage attached to an Amplival microscope (Germany) and a monitoring video apparatus. Samples were rapidly cooled to about –180°C to detect the possible formation of clathrate, ice, salt hydrates, and

TABLE 3. Representative Compositions of Te-Bearing Minerals of the Darasun Goldfield (wt %)

Te	S	Pb	Bi	Ag	Au	Total	Stoichiometric composition	Mineral
27.53	4.17	21.79	47.05	-	-	100.54	$PbBi_2Te_2S_2$	Alexite
46.40	-	-	52.07	0.42	0.39	99.28	Bi_2Te_3	Tellurobismutite
21.45			79.08			100.53	Bi_7Te_3	Hedleyite
34.35	0.05	1.21	63.58	-	-	99.19	Bi_4Te_3	Pilsenite
36.92	0.16		62.21			99.29	Bi_2Te_2	Tsumoite
12.45	6.29	-	82.11	-	-	100.85	Bi_4TeS_2	Joseite A
21.48	2.92	0.40	74.34	0.05	-	99.19	Bi_4Te_2S	Joseite B
35.27	4.53	0.53	59.35	0.02	-	99.70	Bi_2Te_2S	Tetradymite
32.25	-	-	-	41.39	25.61	99.25	$AuAg_3Te_2$	Petzite
37.25	-	-	-	62.58	0.17	100.00	Ag_2Te	Hessite
40.67	-	-	41.42	16.64	-	98.73	$AgBiTe_2$	Volynskite

Note: - = below limit of detection

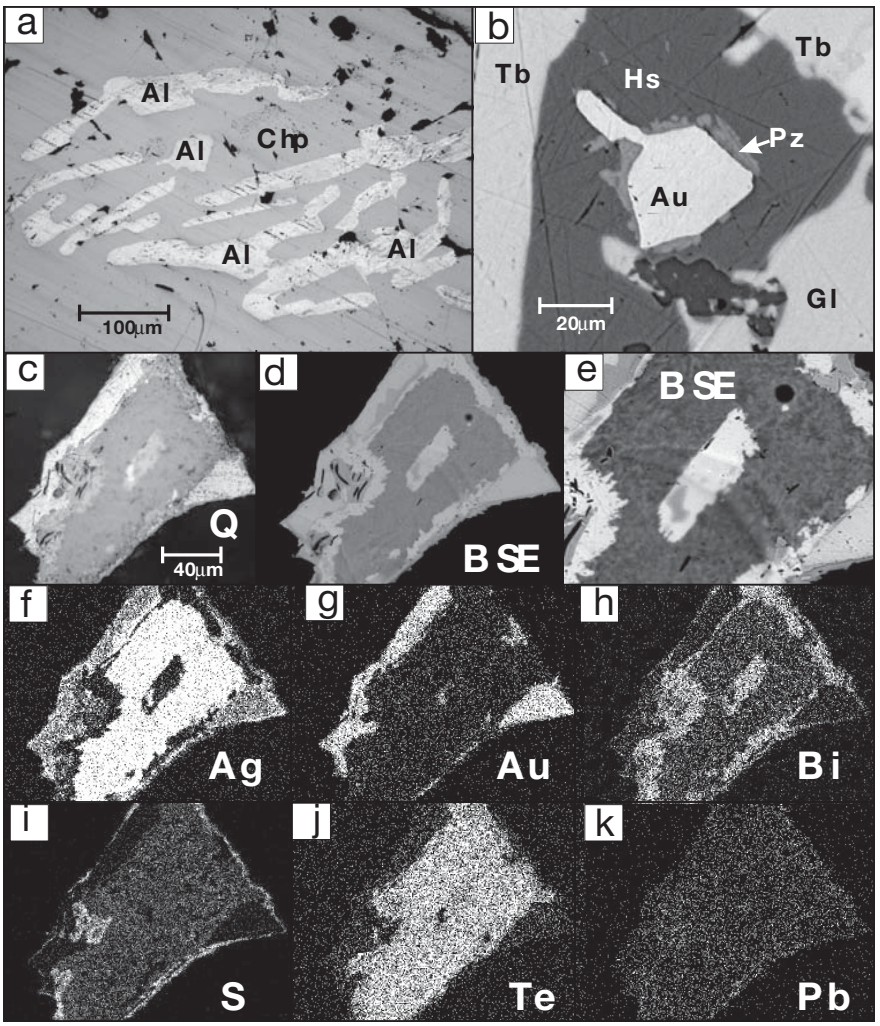

FIG. 9. Photomicrographs of telluride minerals from the Darasun deposit. Images in (a) and (c) are from polished blocks in reflected light, while (b) and (d-k) are BSE images. (a). Probable intergrowth between aleksite (Al) and chalcopyrite (Ccp). (b). Petzite (Pz), hessite (Hs), and tellurobismuthite (Tb) associated with Au. Details of one aggregate of Te, Bi, Ag, and Pb minerals (hedleyite, joseite-B, tetradymite, vikingite) associated with gold and sericite. (c). Reflected light, (d)-(e). BSE images. (f)-(k). Element maps. Other abbreviations: Ccp = chalcopyrite, Gn = galena, Q = quartz.

carbonic solid phase. Upon progressive heating, up to seven phase transitions were observed in the inclusions, namely eutectic melting (T_e), melting of the carbonic phase ($T_{m(CO_2)}$), melting of the ice ($T_{m(ice)}$), clathrate melting ($T_{m(clathrate)}$), homogenization of the carbonic phase ($T_{h(CO_2)}$),, melting of the solid phase ($T_{m(solid)}$), mainly halite, and total homogenization ($T_{h(total)}$). The bulk salinity of the fluid was calculated from the $T_{m(ice)}$ or $T_{m(solid)}$ (Bodnar and Vityk, 1994), or from the combination of $T_{h(CO_2)}$ and $T_{m(clathrate)}$ (Brown, 1989). The identity of the species in solutions was determined from eutectic temperatures (Borisenko, 1977). The pressure of the heterogeneous fluid was estimated from petrographically associated vapor- and liquid-rich inclusions as the sum of the partial pressures of water vapor and CO_2, if present (Brown and Lamb, 1989).

Quantitative chemical analyses of the inclusion fluid were carried out at the Central Institute of Geological Exploration for Base and Precious Metals of Moskow (analyst: Y.V. Vasyuta), using the technique reported by Kryazhev et al. (2006). This is a standardized technique that includes three operations: cleaning of the sample, opening of the fluid inclusions, and element quantification. The analyzed samples were 0.5- to 1.0-g aliquots of milled quartz (0.25- to 0.5-mm sieved fraction), which were cleaned using concentrated (50 vol %) HNO_3 solutions and electrolytic streaming of H_2O (Roedder, 1958). Additional cleansing was achieved with ultrasonic cleaners. Before analysis, samples were brought to dryness and then placed in a single-shot reactor that was filled with helium and preheated at 110°C. Subsequent heating to 400°C and milling with corundum beads (but at a T of about 120°C) allowed the complete opening of the inclusions. The extracted gas phase was analyzed using a Tsvet-100 gas chromatograph to determine the concentration of water, CO_2, methane, and other gases possibly present. The residual liquid phase was analyzed by ion chromatography (Tsvet-3006, for determination of Cl, F, SO_4, and NO_3, sensitivity 0.01 mg/l) and ICP-MS (Elan-6100) after centrifugation and addition of 7 ml of ultrapure deionized water. Measurements by

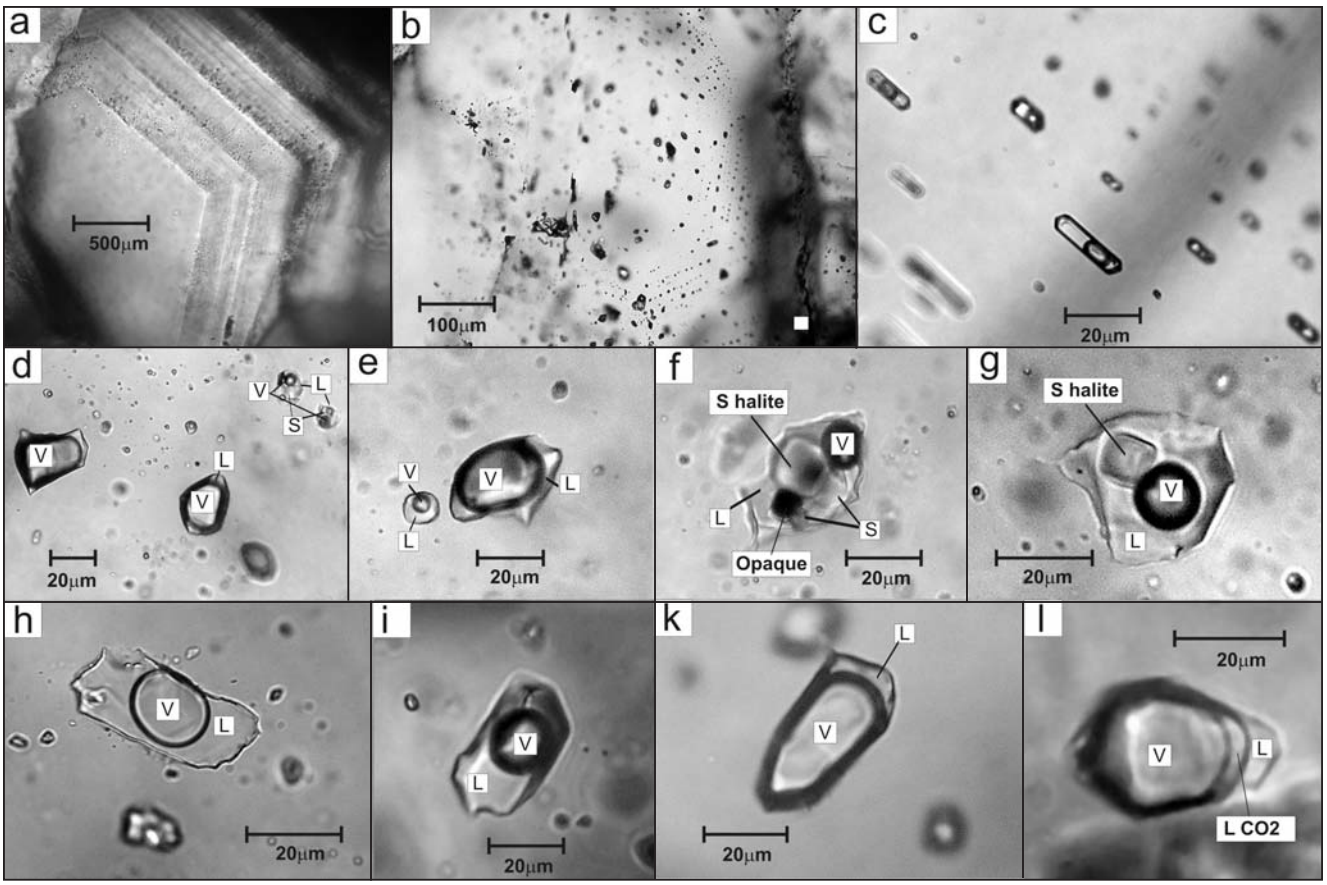

FIG. 10. Fluid inclusions in quartz from the Darasun district deposits. (a). Zoned quartz with tens of growth bands marked by primary FIAs (Darasun). (b). Detail of a growth band hosting both fluid types (1) and (2) (Darasun). (c). L-V, type (2) inclusions from a growth band of early-stage quartz (Teremkyn). (d). Coexisting type (3) and type (1) inclusions within quartz (Talatui). (e). Coexisting type (3) and type (2) inclusions (Darasun); details of multiphase type (1) inclusions from Talatui (f) and Darasun (g); details of type (2) inclusions from Darasun (h) and Talatui (i); (k, l) details of L-V FIAs (k: Teremkyn; l = Talatui, note the presence of L and V CO_2). L = liquid, S = crystal phase of chloride (halite and others), V = vapor.

ion chromatography are accurate within about 5 percent, whereas those carried out by ICP-MS show an accuracy that varies from 0.5 to 2 percent, depending on elements present.

The 24 analyses presented here (Table 5) are all from quartz and refer to 12 samples from Darasun, eight from Teremkyn, and four from Talatui. The samples from Darasun and Teremkyn contain only the main-stage ore fluid, whereas those of Talatui contain mixed contributions of early- and main-stage fluids. Because of this, these chemical data provide limited constraints on the evolution of the ore fluid composition with time. Despite these limitations, however, the database provides important insights into the fluid composition; and hence into the minerogenetic history of the district.

Microthermometric data

Darasun deposit: From this deposit, we selected 962 fluid inclusions hosted by early-stage quartz, main-stage sphalerite, quartz, and anhydrite, and late-stage quartz and calcite (Table 4). Figures 11a, d, g and 12a-b report the most important results for the three paragenetic stages and for the three fluid types, allowing the definition of fluid evolution with time. Early-stage quartz contains fluid types (1), (2), and (3), which have substantially different bulk properties (Fig 11a). Fluid type (1) in particular shows a range of T_e from –62° to –52°C (Table 4), which suggests at least the presence of species like NaCl and $CaCl_2$ in the inclusions. This is consistent with the identification of halite crystals by petrographic observations and with the identification of hydrohalite during the freezing experiments. The $T_{h(total)}$ of type (1) inclusions within early quartz occurs in the 230° to 412°C range to the liquid state (Figs. 11a, 12a), and its bulk salinity is 29.3 to 44.8 wt percent NaCl equiv (Figs. 11a, 12b). The bulk density of such fluid varies from 0.89 to 1.08 g/cm^3. All type (2) inclusions within early quartz homogenize also to the liquid state but in the 280° to 399°C range (Fig. 11a). They have a calculated bulk salinity of 1.4 to 24.1 wt percent NaCl equiv and a bulk density of 0.88 to 1.04 g/cm^3. The CO_2-bearing, type (3) inclusions within the early quartz show ranges of $T_{h(total)}$ that are similar to those of fluid type (2), being equal to 290° to 429°C (Figs. 11a, 12a), but homogenization here occurs exclusively to the vapor state. The bulk salinity of type (3a) inclusions is in the range 0.7 to 21.3 wt percent NaCl equiv (Figs. 11a, 12a). Some of these inclusions contain low-density CO_2 (i.e., type 3b fluid, bulk ρ = 0.22–0.77 g/cm^3) that homogenize between –40.0° and +24.7°C via bubble- or dew-point transition. In these inclusions, $T_{m(CO_2)}$ occurs from –59.0° to

TABLE 4. Summary of Microthermometric Data

Mineral	Incl. type	No.[1]	T_h (°C)	T_h (mode)	T_e (°C)	$T_{m(CO_2)}$ (°C)	$T_{h(CO_2)}$ (°C)	$T_{h(CO_2)}$ (mode)	$T_{m(clathrate)}$ (°C)	Wt % NaCl equiv	ρ (g/cm^3)
						Darasun					
						Early stage					
Qtz	(1) S-L-V	32	230–412	Liquid	–52 to –62					29.3–44.8	1.08–0.89
Qtz	(2) L-V	376	280–399	Liquid	–22 to –52					1.4–24.1	1.04–0.88
Qtz	(3a) V-rich	92	290–429	Vapor	–27 to –31					0.7–21.3	0.35–0.20
Qtz	(3b) V-rich	63	311–366	Vapor	–28 to –31	–56.6 to –59.0	24.7 to –40.0	Liq. to Vap	9.1 to 5.1	2.6–15.9	0.77–0.03
						Main stage					
Sph	(2) L-V	117	160–383	Liquid	–27 to –54					0.7–16.8	0.98–0.70
Qtz	(2) L-V	207	210–340	Liquid	–25 to –63					2.2–22.0	0.97–0.66
Anh	(2) L-V	18	214–247	Liquid	–38 to –40					14.8–15.5	0.97–0.94
						Late stage					
Qtz	(2) L-V	52	124–223	Liquid	–25 to –53					2.2–17.0	1.04–0.90
Calc	(2) L-V	5	209	Liquid	–38					10.9	0.94
						Teremkyn					
						Early stage					
Qtz	(1) S-L-V	23	295–466	Liquid	–55 to –68					27.8–41.0	1.10–0.88
Qtz	(2) L-V	507	300–438	Liquid	–22 to –58					3.7–26.2	0.99–0.47
Qtz	(3a) V-rich	270	320–443	Vapor	–20 to –29					2.6–8.0	0.48–0.02
Qtz	(3b) V-rich	63	343–432	Vapor	–20 to –29	–56.8 to –58.2	11.5 to –53.0	Vapor	8.6 to 8.0	1.2–8.1	0.14–0.02
						Main stage					
Qtz	(2) L-V	120	216–298	Liquid	–28 to –58					4.2–26.3	0.99–0.82
						Late stage					
Qtz	(2) L-V	61	118–195	Liquid	–27 to –58					2.6–27.8	1.10–0.89
						Talatui					
						Early stage					
Qtz	(1) S-L-V	41	402–611	Liquid	–35 to –62					56.3–29.9	1.25–0.78
Qtz	(2) L-V	6	469–495	Liquid	–35 to –42					6.0–15.4	0.54–0.49
Qtz	(3a) V-rich	12	431–589	Vapor	–36 to –54					6.0–33.8	0.57–0.02
Qtz	(3b) V-rich	16	440–502	Vapor	–35 to –55	–56.7 to –58.9	31.0 to –49.3	Vapor	-		
						Main stage					
Qtz	(1) S-L-V	97	269–397	Liquid	–36 to –61					30.3–47.1	1.21–0.97
Qtz	(2) L-V	105	273–438	Liquid	–22 to –61					0.7–23.2	0.91–0.47
Qtz	(3a) V-rich	22	342–377	Vapor	–30 to –38					6.6–13.6	0.22–0.20
Qtz	(3b) V-rich	40	292–358	Vapor	–26 to –55	–56.6 to –59.0	24.7 to –40.0	Vapor	8.6 to 7.9	0.9–17.6	0.42–0.03
						Late stage					
Qtz	(2) L-V	18	133–251	Liquid	–21 to –30					0.4–5.4	1.03–0.88
Calc	(2) L-V	19	146–231	Liquid	–28 to –35					0.7–2.1	0.94–0.83

[1] = number of inclusions

–56.6°C and $T_{m(clathrate)}$ between 9.1° and 5.1°C, indicating the presence of a small fraction of other gas components in the fluid (probably <5 mol %). The pressure of this fluid type is estimated within the 11 to 156 MPa range.

Main-stage sphalerite, quartz, and anhydrite (Fig. 11d) contain only fluid type (2). Within sphalerite, these inclusions homogenize to the liquid state at 160° to 383°C, have a bulk salinity that varies between 0.7 and 16.8 wt percent NaCl equiv, and a bulk density of 0.70 to 0.98 g/cm^3. Fluid inclusions in quartz are very similar to those of sphalerite, as they homogenize to the liquid state at 210° to 340°C, have bulk salinities in the 2.2 to 22.0 wt percent NaCl equiv range, and a fluid density from 0.66 to 0.97 g/cm^3. Type (2) inclusions in anhydrite show relatively well defined properties, characterized by $T_{h(total)}$ within the narrow 214° to 247°C range (homogenization to the liquid state), bulk salinity between 14.8 and 15.5 wt percent NaCl equiv, and the bulk density from 0.94 to 0.97 g/cm^3.

Late-stage quartz and calcite host also type (2) inclusions (Fig. 11g), which in quartz homogenize to the liquid state at 124° to 223°C, have a bulk salinity of 2.2 to 17.0 wt percent NaCl equiv, and a bulk density of 0.90 to 1.04 g/cm^3. The few determinations we carried out with the late-stage calcite (Fig. 11g) showed type (2) fluid inclusions with a bulk salinity of

TABLE 5. Physical-Chemical Properties and Some Component Concentrations of the Ore Fluid of the Darasun District (mol %, except as noted)

	Darasun (12)		Teremkyn (8)		Talatui (4)	
Parameter	Max-min	Mean	Max-min	Mean	Max-min	Mean
T_{fluid} (°C)	430–120		466–118		611–133	
P_{fluid} (MPa)	156–11		41–7		117–36	
Wt % NaCl equiv	42.4–0.7		40.6–1.2		56.3–0.4	
CO_2	4.04–0.10	1.72	1.23–0.26	0.88	1.68–0.40	0.82
CH_4	0.78–0.01	0.26	0.33–5 10^{-3}	0.069	0.03–2 10^{-3}	0.02
Cl	0.80–0.08	0.51	1.32–0.19	0.585	6.99–3.37	4.40
HCO	12.29–0.09	2.9	7.1–0.07	2.43	2.04–0.01	1.29
Na	3.95–0.56	1.13	1.90–0.35	0.85	3.55–2.67	0.046
K	3.95–0.27	0.57	0.04–0.04	0.194	1.18–0.87	1.09
Ca	4.83–4 10^{-3}	0.69	2.74–0.02	0.788	1.49–0.46	0.83
Mg	1.55–7 10^{-3}	0.21	0.60–5 10^{-3}	0.256	0.165–0.06	0.12
Br	0.01–2 10^{-4}	5 10^{-3}	9 10^{-3}–2 10^{-4}	6 10^{-3}	0.03–4 10^{-3}	0.015
As	0.06–5 10^{-4}	9.9 10^{-3}	0.02–5 10^{-4}	6 10^{-3}	0.01–3 10^{-3}	8 10^{-3}
B	0.21–1.7 10^{-3}	0.055	0.71–0.013	0.17	0.21–0.02	0.08
Sr	0.01–2 10^{-4}	4 10^{-3}	0.014–1.8 10^{-4}	3.9 10^{-3}	0.02–0.01	0.015
Ba	5 10^{-3}–3 10^{-5}	6.4 10^{-3}	4 10^{-3}–3 10^{-5}	1.5 10^{-3}	0.01–2 10^{-3}	7.4 10^{-3}
Cu	0.12–3 10^{-5}	0.045	0.036–6 10^{-4}	6 10^{-3}	4 10^{-3}–3 10^{-3}	4 10^{-3}
Zn	0.09–5 10^{-5}	0.03	0.08–1 10^{-3}	0.02	0.05–0.02	0.03
Mn	0.02–3 10^{-4}	4 10^{-3}	0.04–3 10^{-4}	0.01	0.16–0.06	0.105
Fe	0.17–1.6 10^{-3}	0.04	0.19–1 10^{-3}	0.035	0.03–8 10^{-3}	0.02
Rb	2 10^{-3}–1 10^{-5}	4 10^{-4}	6 10^{-4}–4 10^{-5}	2.5 10^{-4}	0.003–0.001	2 10^{-3}
Li	0.037–9 10^{-4}	0.01	0.02–1.6 10^{-3}	0.011	0.01–6 10^{-3}	0.01
Cs	1.5 10^{-4}–1 10^{-6}	3 10^{-5}	3.5 10^{-4}–2 10^{-5}	1 10^{-4}	1 10^{-4}–2 10^{-4}	5 10^{-4}
Mo	6.5 10^{-4}–1 10^{-5}	1 10^{-4}	1 10^{-3}–5 10^{-5}	3 10^{-4}	2 10^{-4}–1 10^{-5}	7 10^{-5}
Ag	9 10^{-5}–1 10^{-6}	3 10^{-5}	7 10^{-4}–4 10^{-6}	2 10^{-4}	4 10^{-5}–1.5 10^{-6}	1.5 10^{-5}
Sb	0.07–1 10^{-5}	7 10^{-3}	4 10^{-3}–1 10^{-5}	5 10^{-4}	4 10^{-4}–7 10^{-5}	1 10^{-5}
Cd	2 10^{-4}–1 10^{-6}	4 10^{-5}	4 10^{-4}–1 10^{-5}	1 10^{-4}	2 10^{-4}–1 10^{-4}	1 10^{-4}
Pb	0.001–1 10^{-6}	3 10^{-4}	9 10^{-4}–5 10^{-6}	3 10^{-4}	4 10^{-4}–6 10^{-5}	3 10^{-4}
Bi	5 10^{-5}–2 10^{-7}	1 10^{-5}	1 10^{-4}–3 10^{-7}	4 10^{-5}	2 10^{-6}–5 10^{-7}	1.6 10^{-6}
Co	7 10^{-5}–6 10^{-6}	5 10^{-5}	3 10^{-4}–5 10^{-6}	6 10^{-5}	9 10^{-5}–2 10^{-5}	5 10^{-5}
Ni	9 10^{-4}–2 10^{-5}	7 10^{-4}	7 10^{-3}–1 10^{-4}	1 10^{-3}	4 10^{-4}–3 10^{-4}	3.6 10^{-4}
Te	2 10^{-4}–1 10^{-6}	4 10^{-5}	2 10^{-5}–4 10^{-6}	1 10^{-5}	8 10^{-6}–9 10^{-6}	9 10^{-6}
Au	1 10^{-5}–1 10^{-7}	3 10^{-6}	2 10^{-5}–7 10^{-7}	6 10^{-6}	3 10^{-6}	3 10^{-6}
Hg	4 10^{-6}–2 10^{-6}	5 10^{-6}	8 10^{-6}–3 10^{-7}	5 10^{-6}	1 10^{-5}–2.5 10^{-6}	6 10^{-6}
Tl	1 10^{-5}–5 10^{-7}	4 10^{-6}	8 10^{-6}–2 10^{-6}	5 10^{-6}	5 10^{-5}–1 10^{-5}	3 10^{-5}
Na/K (wt %)	19.7–0.26	6.2	10.5–0.5	3.8	2.5–1.5	1.9
Na/K	16.8–0.22	5.3	9.0–0.4	3.2	2.1–1.3	1.6
Br/Cl (wt %)	0.059–0.003	0.073	0.064–0.006	0.036	0.011–0.002	0.006
Br/Cl	0.026–0.001	0.032	0.028	0.016	0.005–0.001	0.003

Note: Values in brackets in the first row report the number of analyzed samples

about 10.9 wt percent NaCl equiv, a $T_{h(total)}$ at 209°C, and a bulk density of about 0.94 g/cm^3.

Teremkyn deposit: Our database on Teremkyn is based on 1,044 fluid inclusions from early-, main-, and late-stage quartz (Table 4, Figs. 11b, e, h, 12c-d). Similar to the equivalent samples from Darasun, early-stage quartz from Teremkyn hosts fluid types (1), (2), and (3). The data show a range of T_e from –68° to –55°C and $T_{m(hydrohalite)}$ between –0.5° and 0.0°C for fluid type (1), which is compatible with the presence of Mg, Na, and Ca chlorides. Such observation is in agreement also with the petrographic evidence for several cubic crystals with similar refractive index within the inclusions. During the freezing experiments, in some of these inclusions we noticed also the appearance of a crystalline phase (less than 1 μm in size) that melts between –6.1° to 15.2°C. We interpret this phase to be crystalline boric acid (sassolite), and based on the measured T_m and on solubility data for the system H_3BO_3-NaCl-H_2O (Smirnov et al., 2000) we calculate the concentration of boric acid in the fluid to be 40 to 20 g/kg H_2O (or a B concentration of 3,000–7,000 g/t). Inclusion types (1) within early quartz show homogenize into the liquid state in the 368° to 295°C range and have a bulk salinity equal to 28.0 to 41.0 wt percent NaCl equiv (but one inclusion shows $T_{h(total)}$ = 466°C and bulk salinity = 34.0 wt percent NaCl equiv; Figs. 11b, 12c). The corresponding bulk density of this fluid varies between 0.88 and 1.10 g/cm^3. The type (2) inclusions within early quartz homogenize to the liquid state at 300° to 438°C (Fig. 11b), their bulk salinity varies from 3.7 to 26.2 wt percent NaCl equiv, and their bulk density from 0.47 to 0.99 g/cm^3. The type (3a) inclusions within the same quartz homogenize to the vapor state at 320° to 443°C and contain a fluid with a bulk salinity of 2.6 to 8.0 wt percent NaCl equiv (Fig. 11b). Some groups of inclusions within the early quartz contain also type (3b) fluid, which hosts low-density CO_2 (0.02–0.48 g/cm^3) and homogenize to the liquid or vapor state between –53.0° and 11.5°C. The $T_{m\ (CO_2)}$ occurs between –58.2° and –56.8°C, indicating the presence of a small fraction of other

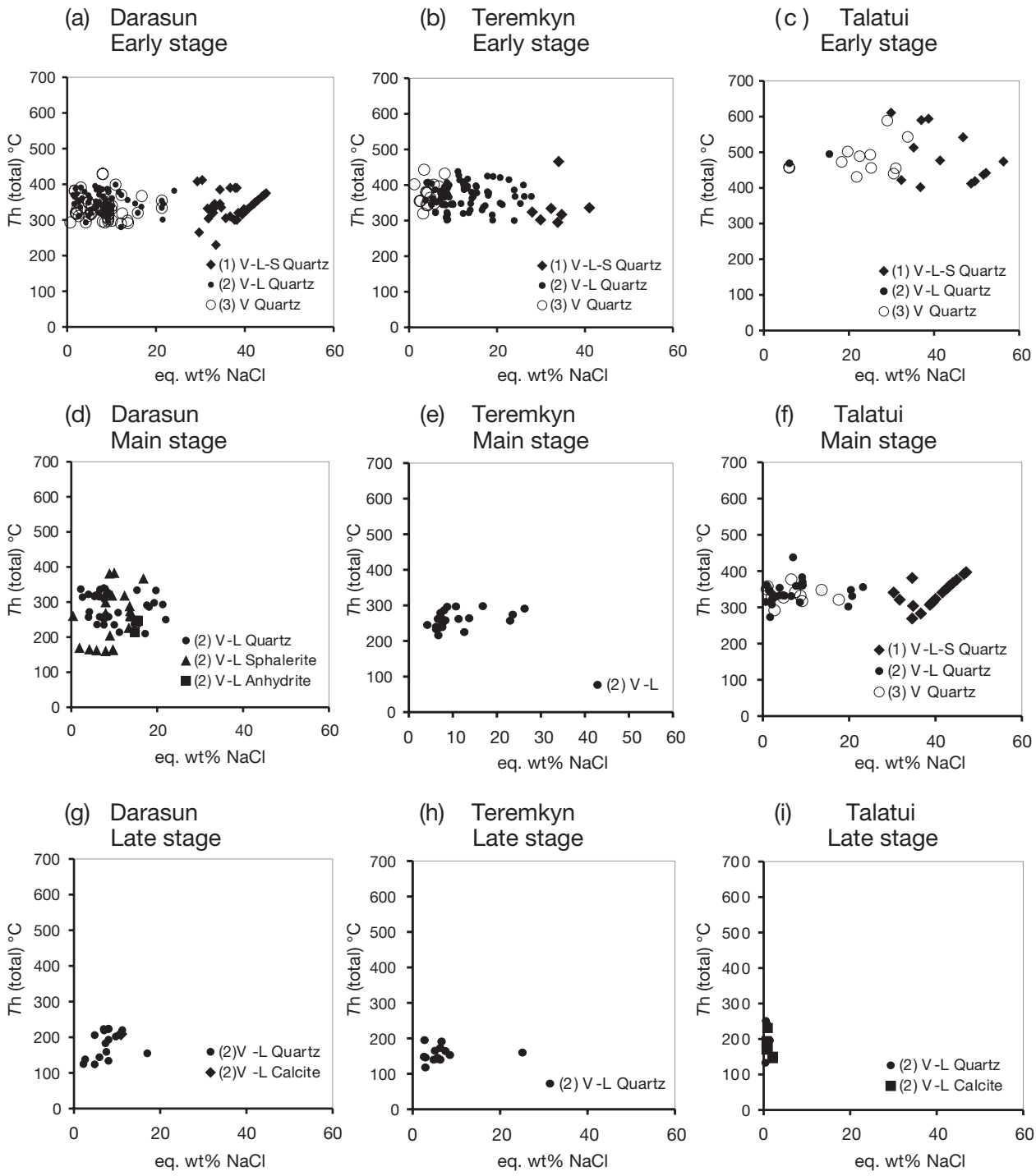

FIG. 11. Total homogenization temperatures vs. equivalent salinities (expressed as wt % NaCl equiv) for different fluid inclusion types and vein minerals of Darasun, Teremkyn, and Talatui.

gases (<5 mol %). For this fluid, we estimate a fluid pressure of 7 to 41 MPa.

Main-stage quartz hosts only type (2) inclusions (Fig. 11e), which homogenize into the liquid state at 216° to 298°C, have a bulk salinity of 4.2 to 26.3 wt percent NaCl equiv, and density of 0.82 to 0.99 g/cm^3. Late-stage quartz hosts also only type (2) inclusions (Fig 11h), but their $T_{h(total)}$ varies between 118° and 195°C, and all homogenization occurs into the liquid state. For these inclusions, bulk salinities vary from 2.6 to 27.8 wt percent NaCl equiv and the bulk density from 0.89 to 1.10 g/cm^3.

Talatui deposit: From this deposit we analyzed 376 fluid inclusions entrapped within early-, main-, and late-stage quartz, and late-stage calcite (Table 4, Figs. 11c, f, I, 12e-f). Similar

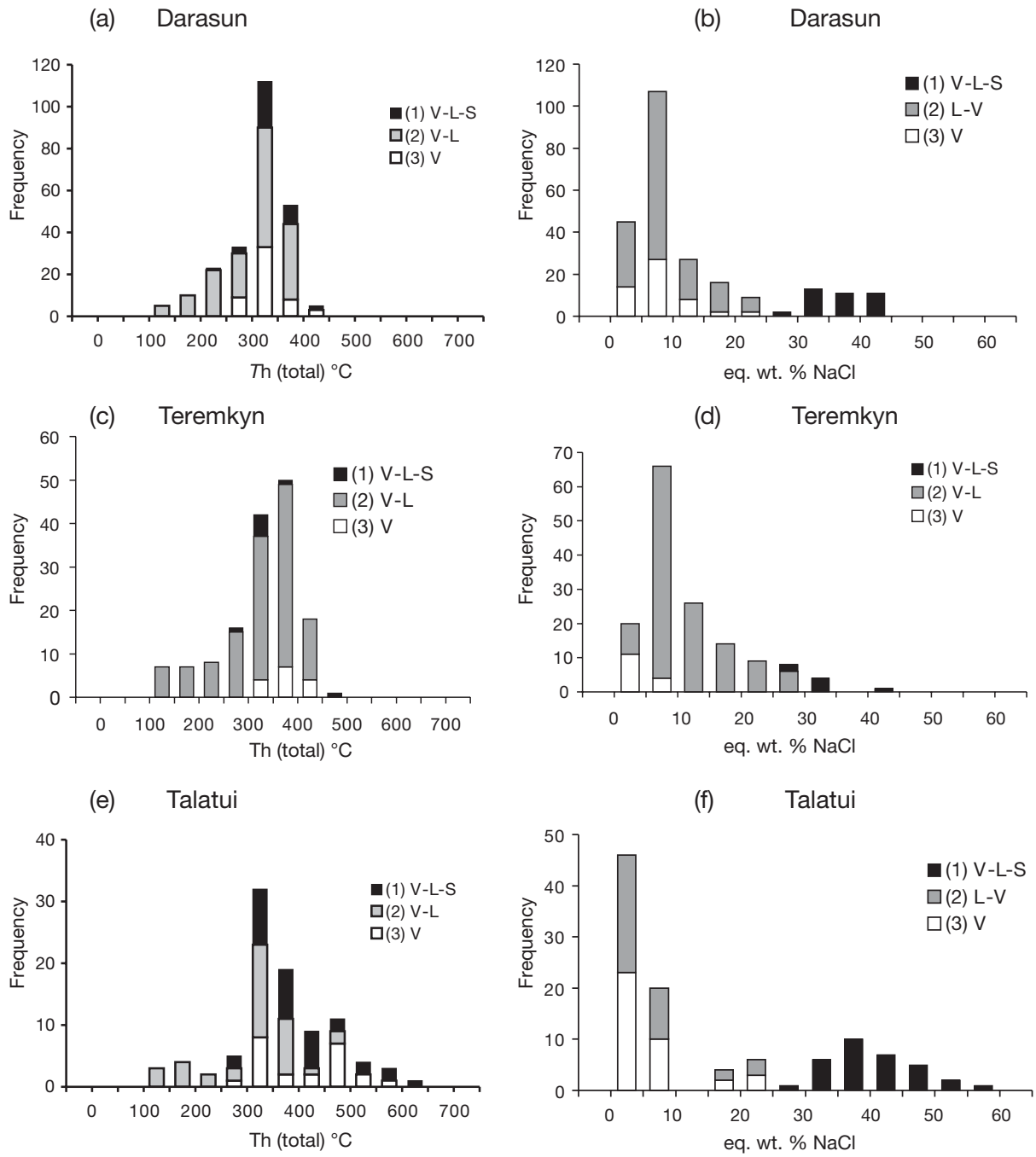

FIG. 12. Cumulative histograms of total homogenization temperatures and equivalent salinities of the different fluid inclusion types of Darasun, Teremkyn, and Talatui.

to the corresponding samples from Darasun and Teremkyn, early-stage quartz from Talatui hosts fluid types (1), (2), and (3). The T_e documented in type (1) inclusions range from −62° to −35°C and $T_{m(hydrohalite)}$ between −0.5° and 0°C, which indicates the presence of Mg, Na, and Ca chlorides. Type (1) inclusions within early-stage quartz homogenize into the liquid state within the temperature range 402° to 611°C (Figs. 11c, 12e), and their bulk salinity amounts to 29.9 to 56.3 wt percent NaCl equiv (Figs. 11c, 12f). The calculated bulk density varies from 0.78 to 1.25 g/cm^3.

Type (2) inclusions within early-stage quartz show a range of $T_{h(total)}$ of 469° to 495°C, and homogenization takes place exclusively into the liquid state. Bulk salinity varies from 6.0 to 15.4 wt percent NaCl equiv and fluid density from 0.49 to 0.54 g/cm^3. The type (3a) inclusions within the same quartz homogenize instead into the vapor state at 431° to 589°C and have a bulk salinity ranging from 5.9 to 33.8 wt percent NaCl equiv (Figs. 11c, 12e). Similar to Darasun and Teremkyn, some of these inclusions host a low-density CO_2 (fluid type 3b, ρ = 0.02–0.57 g/cm^3), which homogenized into the vapor

state over the interval –49.3° to +31.0°C. These inclusions show a $T_{m(CO_2)}$ between –58.9° and –56.7°C, which indicates also in this case a small fraction of other gases in the fluid (<5 mol %). The pressure estimates for these inclusions are in the range 36 to 117 MPa.

A peculiarity of Talatui (Fig. 11f) is that the main-stage quartz hosts the type (1) brine inclusions in addition to inclusion types (2) and (3). The type (1) homogenizes only to the liquid state within a temperature range of 269° to 397°C and has a bulk salinity of 30.3 to 41.7 wt percent NaCl equiv. The corresponding bulk density varies from 0.97 to 1.21 g/cm^3. The type (2) inclusions homogenize also into the liquid state at 273° to 438°C and their bulk salinity varies from 0.7 to 23.2 wt percent NaCl equiv (ρ = 0.47–0.91 g/cm^3). Type (3a) inclusions homogenize into the vapor state at 342° to 377°C and have a bulk salinity ranging from 6.6 to 13.6 wt percent NaCl equiv. Some of these inclusions contain a low-density CO_2 (fluid type 3b, ρ = 0.03–0.42 g/cm^3) and homogenize into the vapor state between –40.0° and +24.7°C. The $T_{m(CO_2)}$ ranges from –59.0° to –56.6°C, indicating a small fraction of other gases. The pressure estimates for these inclusions are 11 to 73 MPa.

The late-stage quartz and calcite of Talatui host only the type (2) inclusions (Figs. 11i, 12e-f). Within quartz, these inclusions homogenize into the liquid state at 133° to 251°C and have a bulk salinity varying from 0.4 to 5.4 wt percent NaCl equiv (ρ = 0.88–1.03 g/cm^3). Within calcite, these inclusions homogenize in a very similar range ($T_{h(total)}$ = 146°–231°C) and have a similar bulk salinity (0.7–2.1 wt % NaCl equiv, ρ = 0.83–0.94 g/cm^3).

To summarize, petrographic and microthermometric data show a range of fluid associations and phase transitions that vary systematically within the district. While Talatui fluid types (1), (2), and (3) were trapped together during both the early and main stages of deposition, only fluid type (2) was present at Darasun and Teremkyn during main-stage deposition. In these deposits, the CO_2-bearing type (3) fluid occurs exclusively in the early-stage quartz. The range of $T_{h(total)}$ recorded at Talatui for fluid type (1) (Fig. 11c) is at least 100°C higher than that recorded at Darasun and Teremkyn for the same fluid type (equal to 230°–465°C, Table 4, Fig. 11a-b). A similar comparison can be made between the properties of the early-stage type (2) fluid of Talatui and the corresponding ones in the other two deposits. Finally, the documented phase transitions in the three deposits show a systematic distribution of modes of homogenization. Fluid types (1) and (2) entrapped within the early quartz of the three deposits homogenize systematically into the liquid state, whereas the coeval type (3) fluid in the same samples homogenize consistently into the vapor state. The same distribution of homogenization modes is found in the main-stage quartz of Talatui, where the type (3) fluid homogenizes consistently into the vapor state ($T_{h(total)}$ range: 290°–380°C) and type (1) and (2) fluids homogenize into the liquid state within a similar range of temperatures (270°–440°C, Table 4). The late-stage, type (2) vein fluid have ranges of $T_{h(total)}$ and bulk salinities that are systematically lower from those of the paragenetically earlier fluids.

Chemical compositions of the ore-forming fluid

Mass spectrometric and chromatographic data show that the ore fluid belonging to the early and main paragenetic stages of the three deposits is rich in Na and K chlorides, with elevated (in places exceptional) concentrations of Mg, As, Cu, Zn, Pb, Fe, Li, Sb, Te, and REEs (Table 5, Fig. 13). These concentrations show however a peculiar spatial distribution, as they vary systematically from one deposit to the other, i.e., they vary as a function of location within the district. In detail, Cl, Na, K, Cs, Br, Sr, Rb, Mn, and Tl are relatively enriched in the Talatui samples, whereas in contrast CO_2, CH_4, HCO_3^-, Cu, Pb, Fe, Co, and Hg are either enriched in the Darasun and Teremkyn fluids or show no systematic variations. Au concentrations vary between 1 10^{-7} and 2 10^{-5} mol percent (0.01–3 g/t) at Darasun and Teremkyn, whereas at Talatui values do not exceed 3 10^{-6} mol percent (0.4 g/t, Table 5). Similarly, Ag concentrations are systematically lower at Talatui, although absolute values in some samples are very high. Br/Cl ratios show systematic variations as well. At Talatui, a relatively narrow range of Br/Cl ratios is coupled with relatively large variations of chlorine concentration (Fig. 14), whereas at Darasun and Teremkyn the large Br/Cl range is coupled with relatively small variations of Cl concentration (Fig. 13).

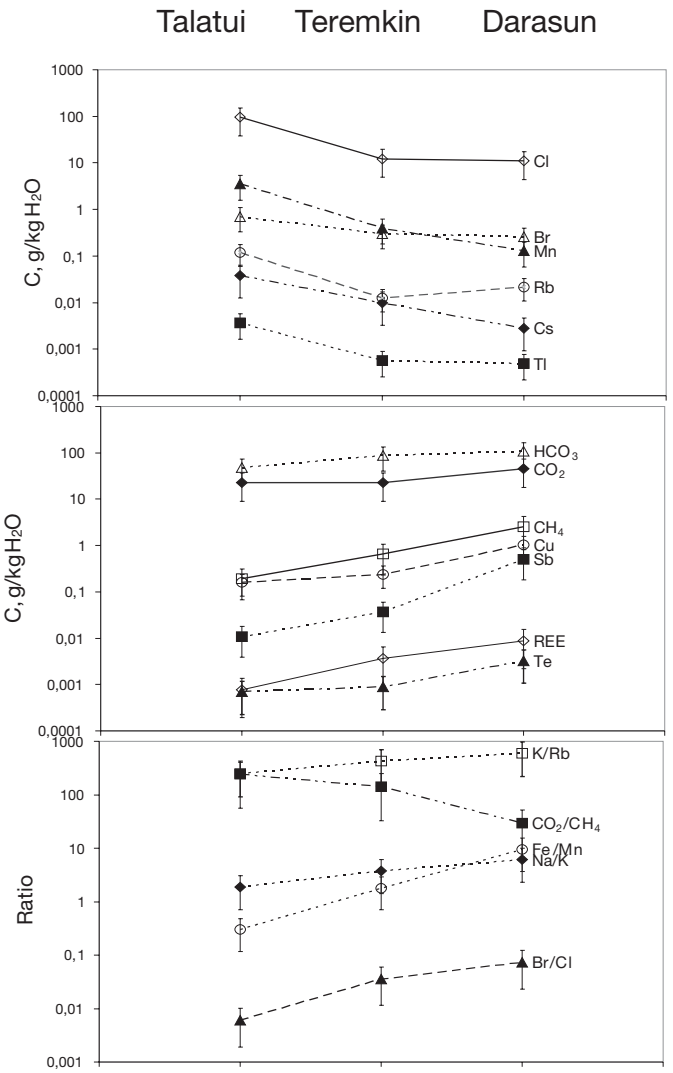

FIG. 13. Comparison between the chemical compositions of the ore-forming fluids of the Darasun district.

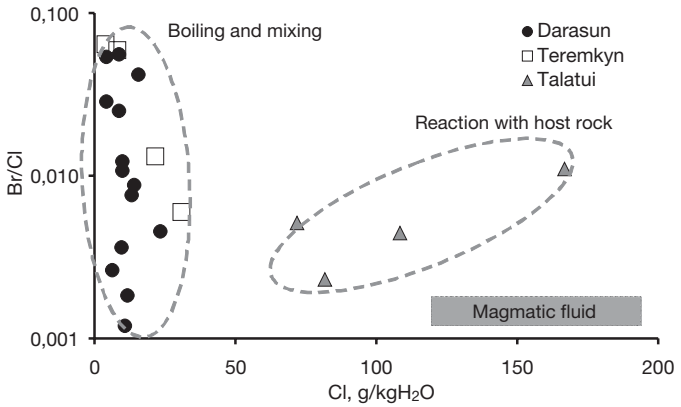

FIG 14. Chlorine concentration vs. Br/CI concentration ratio in the fluid inclusions of the Darasun district. Magmatic Br/Cl ratios from Böhlke and Irwin (1992) and Banks et al. (2000).

All these compositional ranges are primary compositional features of the early- and main-stage ore fluids, as the samples we selected contain no late-stage fluids. One peculiar compositional feature of the ore fluid is instead provided by the concentration ranges of Ni and Sb in the samples. These values are so high (up to hundreds of g/t, Table 5) that they can only be explained by the precipitation of submicroscopic mineral aggregates from a supersaturated fluid within the inclusions.

Discussion and Conclusions

The data presented in this work show that the neighboring Darasun, Teremkyn, and Talatui deposits share fundamental characteristics. They are spatially and temporally related with subduction-related, metal-rich, and oxidized (magnetite-bearing) porphyry stocks and apophyses of dioritic to granitic composition. Their orebodies form veins and ore shoots of variable geometry, contain a Bi-Te-Cu-Ag-Sb-Pb-As-Fe-W metal association, show a variable degree of Au purity, and host a high-temperature, high-salinity ore fluid. The combination of these geological and geochemical characteristics, which were partly discussed in a previous work by Zorin et al. (2001), are consistent with the features described for the intrusion-related class of gold deposits (Sillitoe and Thompson, 1998; Thompson et al., 1999; Lang and Baker, 2001). It must be emphasized that, taken individually, these characteristics are not exclusive of a specific class of gold deposits and may generate misclassifications between intrusion-related and orogenic deposits (cf. Groves et al., 2003). A comprehensive discussion of these features, and especially the extent to which they may be misleading in characterizing intrusion-related gold deposits if considered individually, is not the object of this work. However, we highlight the evidence that all these characteristics are also present at Darasun, which represents a clear difference with respect to other classes of deposits (Table 6) and circumstantial evidence for an intrusion-related affiliation. In the following paragraphs, we discuss our fluid inclusion data and show how a magmatic derivation of the early- and main-stage ore fluid is compatible with the data.

The halide-saturated fluid (type 1 inclusions) homogenizing up to 610°C in the Darasun district (Figs. 10b, d, f, g, 11a-c) is entrapped within euhedral quartz crystals coeval with the first stage of gold precipitation. This paragenetically early ore fluid is ubiquitous within the ore zones and is volumetrically significant if compared with the proportion of the other fluid types in the samples. Such a fluid is not typical of orogenic deposits (Table 6), where a low-salinity, mixed aqueous-carbonic fluid with low to moderate CO_2 contents dominates (Ridley and Diamond, 2000). In the well-studied orogenic deposit of Sigma (Abitibi belt, Canada), a volumetrically minor aqueous fluid with variable bulk salinity (mostly in the range 5–20 wt % NaCl equiv) and $T_{h(total)}$ generally below 350°C was documented together with the typical aqueous-carbonic fluid (Boullier et al., 1998), but this fluid was interpreted as a product of occasional phase separation (from a parent aqueous-carbonic fluid) and not an early-stage ore fluid. Preliminary LA-ICP-MS data on inclusions hosting this Au-bearing aqueous fluid of Sigma (Garofalo, 2000; Garofalo et al., 2002) show the predominance of Na (3,900–31,000 g/t) and K (380–9,500 g/t) ions in the fluid, which is in strong contrast with the data presented here on the high-temperature brines of Darasun, Teremkyn, and Talatui (Table 5), showing alkaline earth metals and transition metals in high concentrations in the fluid together with alkaline metals. Aqueous chloride brines (either super- or undersaturated with respect to halides) with properties similar to those documented here are considered typical of shallow intrusion-related Au deposits (corresponding to pressures of 150 MPa or less: Lang and Baker, 2001). Shallow conditions of mineralization are those estimated for Darasun (10–160 MPa, Table 5).

The early- and main-stage, CO_2-bearing fluid type (3) documented in the district (Fig. 10l, Table 4) shows ranges of CO_2 concentrations (X_{CO_2} = 0.001–0.06), bulk salinities (1–35 wt % NaCl equiv), and $T_{h(total)}$ (300°–590°C) that are consistent with those described for intrusion-related deposits (Lang and Baker, 2001). In orogenic deposits of demonstrated metamorphic origin, e.g., those of the Central Iberian zone of Spain (Murphy and Roberts, 1997), the aqueous-carbonic fluid that forms the deposit has in general a higher CO_2 concentration (X_{CO_2} = 0.02–0.10), a much narrower range of salinities (<6 wt % NaCl equiv), and a definitively lower range of $T_{h(total)}$ (250°–380°C). Thus, the overall compositional characteristics of the ore fluids in the Darasun district suggest a magmatic component during the early and main stages of mineral precipitation and a magmatic derivation of gold itself. This agrees with the magmatic $\delta^{18}O$ = 4.6 to 9.2 per mil of the ore fluid calculated from the oxygen isotope composition of paragenetically early tourmaline and carbonates from Darasun (Prokof'ev et al., 2000).

Useful considerations on the mechanisms of Au deposition in the three deposits can be made from the microthermometric properties of type (1), (2), and (3) fluid inclusions within the vein minerals. At the scale of individual deposits, these fluid types show systematic distributions of $T_{h(total)}$ and bulk salinities. At Darasun all these fluid types occur together within the early-stage quartz (Fig. 10b) and homogenize in a common range between about 300° and 410°C (Fig. 11a). The modes of homogenization and the salinity distributions are however distinct, as the inclusions of fluid types (1) and (2) homogenize into the liquid state, whereas those of fluid type (3) homogenize only into the vapor state. Also, the salinity range of the type (1) fluid (29–45 wt % NaCl equiv)

TABLE 6. Comparison between the Principal Characteristics of Relevant Classes of Au Deposits and Those of the Darasun District

Deposit type	Tectonic setting	Magmatic host	Metal Suite	Mineralization style	Fluid types	T and P	Source
Orogenic	Along deformed continental margins, proximal to trans-crustal lineaments that juxtapose distinct terranes	Mafic and ultramafic volcanic, granitoid intrusions; however, no consistent association between orebodies and granitoid intrusions	Au-Ag±As-Bi-Sb-Te-W. Au fineness: >900	Moderate to steeply dipping veins confined within steeply plunging shear zones; also saddle reefs and disseminations as replacement of Fe-rich host rocks	System: H_2O-NaCl-CO_2-CH_4 X_{CO_2} = 0.1 – 0.25; three fluid types: Aquo-carbonic (3–7 wt % NaCl equiv), aqueous CO_2-poor (less defined), carbonic (X_{CO_2} >0.95); cation abundance: Na>K>Ca>Mg	350° ± 50°C 150 ± 50 MPa	1, 2
Intrusion-related	Above or within old (typically cratonic) magmatic provinces formerly known for W and/or Sn deposits; most deposits occur inboard of convergent plate boundaries; no single tectonic regime typical	From oxidized (magnetite-bearing) to reduced (ilmenite-bearing) alkaline and calc-alkaline hosts; multiple intrusions overlap temporally and spatially in the deposit areas; close association between intrusions and orebodies	Au-Bi±Te-As-Mo-W-Sb-Cu	Sheeted and replacement veins, breccias associated with dikes and sills, and disseminations; distal portions of deposits: contact skarns and replacements in calcareous schists; proportion of sulfides: <5 vol %	System: H_2O-NaCl-CO_2-CH_4 High CO_2 concentration typical, but no quantification reported; two fluid types: CO_2-rich fluid (2–10 wt % NaCl equiv) and aqueous fluid (5–40 wt % NaCl equiv)	200°– 600°C 50–300 MPa	3, 4
Darasun area	Permian-Early Jurassic active margin of Siberia	Oxidized (magnetite-bearing) calc-alkaline and subalkaline granites and granodiorites of the Amudzhikan-Sretensky complex Age: 109–193 Ma	Au-Ag±As-Pb-±Zn-Cu-Te-Sb-Bi±In±Cd±Se±Tl ±Ga. Au fineness: 590–997	Sheeted veins, breccias, and disseminations closely associated with the igneous complex; age: 100±18 Ma; ores contain up to 50 vol % sulfides	System: H_2O-CO_2-NaCl-CH_4; two fluid types: aqueous fluid (0.4–56 wt % NaCl equiv), and vapor (CO_2)-rich; cation abundance: Na~K~Ca~Mg	210°–610°C 10–160 MPa	This study, ref. therein

Note: Sources: 1 = Groves et al. (2003), 2 = Ridley and Diamond (2000), 3 = Lang and Baker (2001), 4: Thompson et al. (1999)

contrasts with that of fluid types (2) and (3) (which are similar, equal to about 1–24 wt % NaCl equiv). Equivalent considerations can be made on the data from type (1), (2), and (3) inclusions of the early-stage quartz of Teremkyn and Talatui (Figs. 10d, 11b-c), for type (1) and (2) inclusions of the main-stage quartz, sphalerite, and anhydrite of Teremkyn and Talatui (Fig. 11de), and also for type (1), (2), and (3) inclusions of the main-stage quartz of Talatui (Fig. 11f).

The petrographic evidence for the contemporaneous entrapment of fluid types (1) and (3), and types (2) and (3) within the same mineral growth zones during precipitation of vein sulfides and gold, the evidence for opposite modes of homogenization of these fluid types within the same range of temperatures, and the systematic distribution of the densities of liquid- and vapor-rich fluid inclusions (Fig. 15) suggest that phase separation (boiling) of the ore fluid could have been an important process at Darasun and Teremkyn. These three types of observations are essential to demonstrate phase separation during a geologic process (Ramboz et al., 1982; Bodnar et al., 1985; Diamond, 2003); however, because we do not report our results here at the scale of individual fluid inclusion assemblages (see Method section), we cannot estimate the exact starting conditions of this process and also how much the properties of the three ore fluids changed as a result of this process. With these limitations, the circumstantial evidence reported above indicates that the ore fluid of Darasun and Teremkyn could have been trapped at various stages within a range of phase separation conditions. Also, petrographic evidence for little or no deformation of the host minerals (Fig. 8c, e, g-h) suggests that postentrapment reequilibration of fluid inclusions must have had a negligible effect on the distribution of the fluid properties (cf. Bodnar, 2003); therefore, our conclusion is not biased by a postentrapment artifact. This is in agreement with the measured Br/Cl ratios in the fluid inclusions (Fig. 14), which reflect a relatively higher fractionation of bromine into the vapor phase at Darasun and Teremkyn due to phase separation, and only a minor fractionation at Talatui (cf. Böhlke and Irwin, 1992; Liebscher et al., 2006).

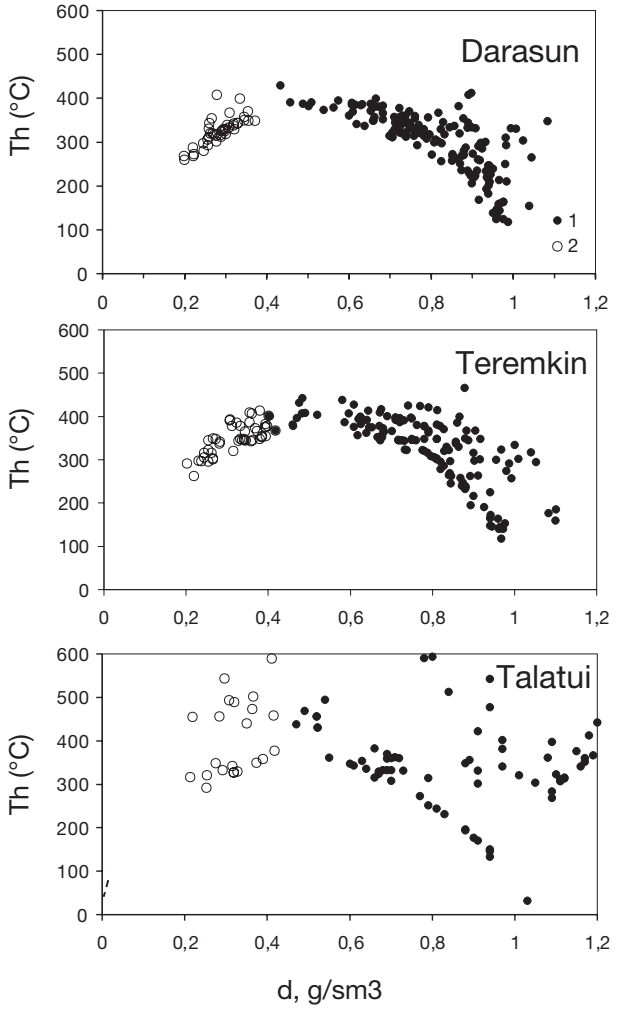

FIG 15. Total homogenization temperature vs. density of the type (2) fluid inclusions entrapped within the main-stage quartz of the Darasun district deposits. Open symbols show the properties of V-rich inclusions, while filled symbols show those of L-rich inclusions. Note that V-rich inclusions plot systematically along the low-density side of the diagram, and L-rich inclusions along the high-density side. Fluid densities calculated using the equation of state of Anderko and Pitzer (1993).

From the cogenetic type (3) and type (1) early-stage inclusions of the three deposits, we estimate that phase separation took place at about 300° to 450°C and 10 to 160 MPa at Darasun and Teremkyn, which corresponds to a depth of mineralization of 1 to 2.5 km. These estimates are semiquantitative evaluations of the entire range of phase separation temperatures and not a record of a single, discrete event. Similarly, the bulk salinities of fluid types (1) to (3) (Fig. 12b, d) provide only a semiquantitative record of the fractionation of chemical species within the vapor and liquid phases of the ore fluid during the entire phase separation stage in the district. Phase separation is known to be very effective in precipitating Au in several geologic environments, due to the fractionation of S or Cl of the thio- and chloride complexes of gold into the vapor phase and their consequent thermodynamic instability (Seward, 1989). We suggest that in the Darasun district this process controlled early gold precipitation, determining therefore the properties of the ore fluid at the later cooling and condensation stages. Gold transport in chloride complexes was most probable at the early stages of the deposit formation, whereas the Au hydrosulfide complexes prevailed at the main stages. Another process that must have controlled gold precipitation was the generation of a CO_2-bearing fluid after the degassing of the magmatic source, which is now entrapped as a high-temperature, CO_2-bearing aqueous fluid (type 3b inclusions). Degassing, which is common in intrusion-related deposits (Lowenstern, 2001), must have occurred intermittently causing an expansion of the locus of the immiscibility field of the ore fluid (cf. Diamond, 2003) and hence affecting gold transport and precipitation at all stages of deposit formation. In the fluid inclusions we studied, the range of CO_2 concentrations (Table 5) and the abundance of other chemical components explain the range of inclusion properties and the discrepancies with an H_2O-NaCl model fluid (Fig. 15).

The microchemical data based on bulk crushing do not resolve the role played by the individual fluid types and by their liquid and vapor phases during metal transport but provide a

set of first-order constraints in combination with other fundamental data. First, the concentrations of the major fluid components in the analyzed inclusions, i.e., Cu, B, Sb, Bi, Te, and in part As, show ranges of values that are systematically higher at Darasun and Teremkyn (Fig. 13, Table 5). We interpret this difference as a product of phase separation, which occurred scarcely in the high-temperature Talatui ore body hosting the most primitive fluid (Fig. 15) but relatively effectively at the lower temperatures. Products of phase separation could also include the higher proportion of chalcopyrite, tourmaline, arsenopyrite, tellurides, and bismuth minerals in the Darasun and Teremkyn orebodies and the range of Br/Cl ratios in the fluid inclusions (Fig. 14).

Another first-order constraint provided by our dataset is the Au/Cu ratio of the Darasun ore fluid, which can be estimated from the range of gold concentrations in the high-temperature inclusions (up to 0.4 g/t Au at Talatui) and from the corresponding fractions of wt percent of Cu. This ratio (reported as g/t vs. wt %) is equal to a range of values between 15 and 35 at Talatui, and if our interpretation of intrusion-related affiliation is correct, can be compared with the same ratio determined for porphyry systems ($\sim 1 \cdot 10^{-4}$, Ulrich et al., 1999). Considering that the inclusions we studied are poorly affected by postentrapment reequilibration, it is highly probable that the five orders of magnitude difference we determine identify a true compositional characteristic of the ore fluid of Darasun. Following the arguments of Ulrich et al. (1999, 2002), we propose that these Au/Cu ratios were controlled by the fundamental properties of the magmatic source rock of the Darasun district, in particular by its Au/Cu ratio. This is in line with recent results from the most fractionated melt hosting the intrusion-related deposit of Timbarra, Australia (Mustard et al., 2006), which has a Au/Cu ratio of about 80 (range: 20–200). This surprising similarity suggests that high Au/Cu ratios in the ore fluid might be characteristic of intrusion-related gold deposits in general and not just a peculiar feature of the Transbaikal deposits.

Because microchemical data do not allow an exact discrimination between early-, main-, and late-stage ore fluids of the deposits, a detailed reconstruction of the ore fluid evolution during and after the magmatic-hydrothermal stage is not possible here. Thus, the exact conditions at which the base metal sulfide, sulfosalt, sulfoantimonite, adularia, and sericite assemblages formed within the orebodies up to the end of the main stage (e.g., Darasun) cannot be identified, as well as the conditions of precipitation of some sulfides and tellurides during the late stage of ore formation (Talatui). The high concentrations of Pb, Zn, and Fe in the fluid inclusions (from hundreds to thousands of g/t, Table 5), as well as the petrographic evidence for an association between gold and galena (Fig. 8d-e), suggest however that base metals, gold, and probably other ore minerals did not always reach saturation in the ore fluid during the early magmatic-hydrothermal stage, and that a fraction of this fluid was possibly transported through the orebodies and dispersed at lower temperatures into the outer fringes of the deposits. This hypothesis is consistent with the presence of a large galena-sphalerite halo around the Darasun stock and is demonstrated around porphyry copper deposits for which a detailed fluid inclusion record is available (cf. Ulrich et al., 2002). Detailed knowledge of the physical-chemical properties of the Darasun ore fluid as a function of mineral precipitation will constrain better the conditions of late transport and precipitation of ore metals in the district. These features could be used in the future as a strategic field indicator of mineralization in the Darasun district as a whole.

Acknowledgments

This work was carried out within the framework of the UNESCO-IGCP project 540 "Gold-bearing hydrothermal fluids of orogenic deposits" and the Russian RFBR (projects 09-05-00697, 09-05-12037, and 10-05-00354). The authors thank T. Ulrich for discussions and comments on an early version of this work. The comments of two anonymous reviews and the editorial work of Jean Cline improved considerably the early version of the manuscript.

REFERENCES

Anderko, A., and Pitzer, K.S., 1993, Equation-of-state representation of phase equilibria and volumetric properties of the system NaCl-H_2O above 573 K: Geochimica et Cosmochimica Acta, v. 57, p. 1657–1680.

Antipin, V.S., Perepelov, A.B., and Zaikin, V.P., 1985, Cesium-bearing volcanic glass of the Vershino-Darasun region (eastern Transbaikalia): Vulcanology and Seismology, v. 6, p. 33–40 (in Russian).

Bakker, R.J., and Diamond, L.W., 2006, Estimation of volume fractions of liquid and vapor phases in fluid inclusions, and definition of inclusion shapes: American Mineralogist, v. 91, p. 634–657.

Benevolskiy, B.I., 2002, Gold of Russia: Moscow, Geoinformmark (in Russian), 462 p.

Bodnar, R.J., 2003, Re-equilibration of fluid inclusion: Mineralogical Association of Canada Short Course Series Volume 32, p. 213–230.

Bodnar, R.J., and Vityk, M.O., 1994, Interpretation of microthermometric data for H_2O-NaCl fluid inclusions, *in* De Vivo, B., and Frezzotti, M. L., eds., Inclusions in Minerals, Methods and Applications [Siena, Italy, 1994]: Blacksburg, VA, Virginia Tech, Proceedings, p. 117–130.

Bodnar, R.J., Reynolds, T.J., and Kuehn, C.A., 1985, Fluid-inclusion systematics in epithermal systems: Reviews in Economic Geology, v. 2, p. 73–97.

Böhlke, J.K., and Irwin, J.J., 1992, Laser microprobe analyses of Cl, Br, I, and K in fluid inclusions: Implications for sources of salinity in some ancient hydrothermal fluids: Geochimica et Cosmochimica Acta, v. 56, p. 203–225.

Borisenko, A.S., 1977, Cryometric analysis of salt composition in vapor-fluid inclusions in minerals: Geologia and Geofizika, v. 8, p. 16–27.

Bortnikov, N.S., 2006, Geochemistry and origin of the ore-forming fluids in hydrothermal-magmatic systems in tectonically active zones: Geology of Ore Deposits, v. 48, p. 1–22.

Boullier, A.-M., Firdakus, K., and Robert, F., 1998, On the significance of aqueous fluid inclusions in gold-bearing quartz vein deposits from the southwestern Abitibi subprovince, Quebec, Canada: Economic Geology, v. 93, p. 216–223.

Brown, P. , 1989, FLINCOR: A computer program for the reduction and investigation of fluid inclusion data: American Mineralogist, v. 74, p. 1390–1393.

Brown, P.E., and Lamb, W.M., 1989, P-V-T properties of fluids in the system H_2O-CO_2-NaCl: New graphical representations and implications for fluid inclusion studies: Geochimica et Cosmochimica Acta, v. 53, p. 1209–1221.

Diamond, L.W., 2003, Introduction to gas-bearing, aqueous fluid inclusions: Mineralogical Association of Canada Short Course Series Volume 32, p. 101–158.

Fedorov, M.V., Chukhonin, L.P., and Khoreva, B.Y., 1980, Stage of formation of metamorphic and granitic formations in west part of Stanovik region from geological and radiological dates: VSEGEI (Karpinsky Russian Geological Research Institute), Leningrad, 1980, Proceedings, p. 103–107 (in Russian).

Garofalo, P.S., 2000, Gold precipitation and hydrothermal alteration during fluid flow through the vein network of the mesothermal gold deposit of Sigma (Abitibi belt, Canada): Unpublished Ph.D. thesis, Zurich, Swiss Federal Institute of Technology, 246 p.

Garofalo, P.S., Heinrich, C.A., Günther, D., and Pettke, T., 2002, PTX properties of a natural Au-bearing hydrothermal fluid from a multidisciplinary study of fluid inclusions (Sigma deposit - Canada) [abs.]: From Stars to Life, Goldschmidt Conference, 2002, Davos, Switzerland, Abstracts, p. A263.

Goldstein, R.H., 2003, Petrographic analysis of fluid inclusions: Mineralogical Association of Canada Short Course Series Volume 32, p. 1–45.

Gosselin, P., and Dubé, B., 2005, Gold deposits of the world: Distribution, geological parameters, and gold content: Geological Survey of Canada Open File 4895, p. 1–214.

Groves, D.I., Goldfarb, R., Robert, F., and Hart, C.J.R., 2003, Gold deposits in metamorphic belts: Overview of current understanding, outstanding problems, future research, and exploration significance: Economic Geology, v. 98, p. 1–29.

Kazimirovsky, M.E., Plusnin, G.S., Smirnov, V. N., and Fefelov, N.N., 1992, Geochemical peculiarities and absolute age of rocks of nucleus of the Darasun tectonic-magmatic structure: Russian Geology and Geophysics, v. 32, p. 61–72 (in Russian).

Kazimirovsky, M.E., Dril, S.I., and Sandimirova, G.P., 1998, Geochemical evidences of subduction origin of Paleozoic granites of western Stanovaya zone: Metallogeny, oil-and-gas content and geodynamic of North-Asian craton and orogenic belt of its framework: Irkutsk, Vinogradov Institute of Geochemistry, p. 270–272 (in Russian).

Kretz, R., 1983, Symbols for rock-forming minerals: American Mineralogist, v. 68, p. 277–279.

Kryazhev, S.G., Prokofiev, V.Y., and Vasyuta, Y.V., 2006, Application of the ICPMS method for the analysis of ore-forming fluids: Vestnik MGU (Moscow University Geology), Geology Series 4, p. 30–36 (in Russian).

Kulikova, Z.I., Gulina, V.A., and Zorina, L.D., 1996, The role of explosion breccias as indicators in the genesis of the Teremkin gold deposit (eastern Transbaikalia): Geologia and Geofizika, v. 37, p. 61–72 (in Russian).

Kuzmin, M.I., 1985, Geochemistry of magmatic rocks of phanerozoic activic belts: Novosibirsk, Nauka Edition (in Russian), 200 p.

Lang, J.R., and Baker, T., 2001, Intrusion-related gold systems: the present level of understanding: Mineralium Deposita, v. 36, p. 477–489.

Liebscher, A., Lüders, V. , Heinrich, W.G., and Schettler, G., 2006, Br/Cl signature of hydrothermal fluids: Liquid-vapour fractionation of bromine visited: Geofluids, v. 6, p. 113–121.

Lowenstern, J.B., 2001, Carbon dioxide in magmas and implications for hydrothermal systems: Mineralium Deposita, v. 36, p. 490–502.

Lyakhov, Y.V., and Dmitriev, L.K., 1975, Physical-chemical conditions of mineral forming process in Darasun gold deposit (eastern Transbaykalia) from fluid inclusions data: Lvovsky University, Mineralogichesky Sbornic, p. 17–22 (in Russian).

Murphy, P.J., and Roberts, S., 1997, Evolution of a metamorphic fluid and its role in the lode gold mineralization in the Central Iberian zone: Mineralium Deposita, v. 32, p. 459–474.

Mustard, R., Ulrich, T., Kamenetsky, V.S., and Mernagh, T., 2006, Gold and metal enrichment in natural granitic melts during fractional crystallization: Geology, v. 34, p. 84–88.

Pakhol'chenko, Y.A., Zorina, L.D., and Plyusnin, G.S., 1987, First Rb/Sr ages for metasomatites of the Darasun ore field in Transbaikalia: Doklady Akademii Nauk of USSR, v. 295, p. 1219–1223 (in Russian).

Prokof'ev, V.Y., Bortnikov, N.S., and Zorina, L.D., 2000, Genetic features of the Darasun gold-sulphide deposit (eastern Transbaikal region, Russia): Geology of Ore Deposits, v. 42, p. 526–548.

Prokof'ev, V.Y., Zorina, L.D., Baksheev, I.A., Plotinskaya, O.Y., Kudryavtseva, O.E., and Ishkov, Y.M., 2004, Minerals and formation conditions of ores of the Teremkin gold deposit (eastern Transbaikal region, Russia): Geology of Ore Deposits, v. 46, p. 332–352.

Prokof'ev, V.Y., Baksheev, I.A., Zorina, L.D., Belyatskii, B.V., and Bortnikov, N.S., 2006, First estimate of the age of gold ores of the Darasun deposit (eastern Transbaikal region) by the Sm-Nd method: Doklady Earth Sciences, v. 409A, p. 963–966.

Prokof'ev, V.Y., Zorina, L.D., Kovalenker, V. A., Akinfiev, N.N., Baksheev, I.A., Krasnov, A.N., Yurgenson, G.A., and Trubkin, N.V. , 2007, Composition, formation conditions, and genesis of the Talatui gold deposit, the eastern Transbaikal region, Russia: Geology of Ore Deposits, v. 49, p. 31–68.

Prokof'ev, V.Y., Bortnikov, N.S., Volkov, A.V. , Baksheev, I.A., and Zorina, L.D., 2008, Dissiminated ores of the Darasun gold deposit (eastern Transbaikalia) and their genesis: Doklady Earth Sciences, v. 422, p. 1025–1027.

Ramboz, C., Pichavant, M., and Weisbrod, A., 1982, Fluid immiscibility in natural processes: Use and misuse of fluid inclusion data. II: Interpretation of fluid inclusion data in terms of immiscibility: Chemical Geology, v. 37, p. 29–48.

Ridley, J.R., and Diamond, L.W., 2000, Fluid chemistry of orogenic lode-gold deposits and implications for genetic models: Reviews in Economic Geology, v. 13, p. 141–162.

Roedder, E., 1958, Technique for the extraction and partial chemical analysis of fluid-filled inclusions from minerals: Economic Geology, v. 53, p. 235–269.

Rublev, A.G., Alexandrov, G.V., and Alexandrova, S.V., 1985, Geochronology of Phanerozoic activisation magmatism in northeastern Transbaykalia: Sovetskaya Geologia, v. 10, p. 81–92 (in Russian).

Safonov, Y.G., 1997, Hydrothermal gold deposits: Abundance, geological-genetic types, and productivity of ore-forming systems: Geology of Ore Deposits, v. 39, p. 20–32.

Sakharova, M.S., 1968, The gold mineralogy of the Darasun deposit (eastern Transbaikal region): Izvestiya Akademii Nauk USSR, Geology series, v. 11, p. 51–68 (in Russian).

——1969, Mineralogy of Darasun gold field in eastern Zabaykal'ye: International Geology Review, v. 11, p. 45–59.

——1972, Stages of ore formation and zonation in the Darasun gold deposit: Ore formation and its relation to magmatism: Moskow, Nauka, p. 213–222 (in Russian).

Seward, T.M., 1989, The hydrothermal chemistry of gold and its implication for ore formation: Boiling and conductive cooling as examples: Economic Geology Monograph 6, p. 398–404.

Sillitoe, R.H., and Thompson, J.F.H., 1998, Intrusion-related vein gold deposits: Types, tectono-magmatic settings, and difficulties of distinction from orogenic gold deposits: Resource Geology, v. 48, p. 237–250.

Smirnov, S.Z., Peretyazhko, I.S., and Prokof'ev, V. Y., 2000, First finding of sassolite (H_3BO_3) in fluid inclusions in minerals: Russian Geology and Geophysics, v. 41, p. 194–206 (in Russian).

Tauson, L.V., Gundobin, G.M., and Zorina, L.D., 1987, Geochemical fields of ore magmatic systems: Novosibirsk, Nauka (in Russian), 202 p.

Thompson, J.F.H., Sillitoe, R.H., Baker, T., Lang, J.R., and Mortensen, J.K., 1999, Intrusion-related gold deposits associated with tungsten-tin provinces: Mineralium Deposita, v. 34, p. 323–334.

Timofeyevsky, D.A., 1972, Geology and mineralogy of the Darasun gold area: Moskow, Nedra (in Russian), 260 p.

Ulrich, T., Günther, D., and Heinrich, C.A., 1999, Gold concentrations of magmatic brines and metal budget of porphyry copper deposits: Nature, v. 399, p. 676–679.

——2002, The evolution of a porphyry Cu-Au deposit, based on LA-ICP-MS analysis of fluid inclusions: Bajo de la Alumbrera, Argentina: Economic Geology, v. 97, p. 1889–1920.

Yakubchuk, A.S., Shatov, V.V., Kirwin, D., Edwards, A., Tomurtogoo, O., Badarch, G., and Buryak, V. A., 2005, Gold and base metallogeny of the central Asian orogenic supercollage: Economic Geology 100th Anniversary Volume, p. 1035–1068.

Yurgenson, G.A., and Yurgenson, T.N., 1995, Deposits in the Transbaikal region: Moskow, Geoinformmark, p. 3–18 (in Russian).

Zorin, Y.A., Belichenko, Y.A., Rutshtein, I.G., Zorina, L.D., and Spiridonov, A.M., 1998, Geodynamics of the western Mongolian-Okhotsk fold belt and tectonic position of gold occurrences in Transbaikalia: Russian Geology and Geophysics, v. 39, p. 1578–1586 (in Russian).

Zorin, Y.A., Zorina, L.D., Spiridonov, A.M., and Rutshtein, I.G., 2001, Geodynamic setting of gold deposits in eastern and central Trans-Baikal (Chita) region, Russia: Ore Geology Review, v. 17, p. 215–232.

Zorina, L.D., Sanina, N.B., Gulina, V.A., and Andrulaitis, L.D., 1991, Mineralogical-geochemical zonation of the deposit of the gold-quartz-sulfide formation: Geochemical prospecting of ore deposits in Taiga regions: Novosibirsk, Nauka, p. 188–200 (in Russian).